# A review of additive manufacturing of ceramics by powder bed selective laser processing (sintering / melting): Calcium phosphate, silicon carbide, zirconia, alumina, and their composites

David Grossin [a,*], Alejandro Montón [a], Pedro Navarrete-Segado [a,b], Eren Özmen [a,c], Giovanni Urruth [a,d], Francis Maury [a], Delphine Maury [d], Christine Frances [b], Mallorie Tourbin [b], Pascal Lenormand [c], Ghislaine Bertrand [a]

[a] CIRIMAT, Université de Toulouse, CNRS, 4 Allée Émile Monso, 31432 Toulouse Cedex 4, France
[b] Laboratoire de Génie Chimique, Université de Toulouse, CNRS, INPT, UPS, Toulouse, France
[c] CIRIMAT, Université de Toulouse, CNRS, Université Toulouse 3 - Paul Sabatier, 118 Route de Narbonne, 31062 Toulouse cedex 9 - France
[d] Marion Technologies, Parc Technologique Delta Sud, 09340 Verniolle, France

## ARTICLE INFO

## ABSTRACT

This review offers an overview on the latest advances in the powder bed selective laser processing, known as selective laser sintering/melting, of calcium phosphate, silicon carbide, zirconia, alumina, and some of their composites. A number of published studies between 1991 and August 2020 was collected, analyzed and an inclusive state of the art was created for this review. The paper focuses on the process description, feedstock criteria and process parameters and strategy. A comparison is made between direct and indirect powder bed selective laser processing of each ceramic, regarding the present achievements, limitations and solutions. In addition, technical aspects and challenges about how to address these issues are presented.

## 1. Introduction

Ceramics have been used in a wide range of applications due to their various excellent properties, including high mechanical strength and hardness, low thermal conductivity, high wear and corrosion resistance. This makes them appropriate candidate materials for diverse ranges of applications in modern industries, such as aerospace, defense, electronics, automotive, and chemical. Furthermore, some ceramics exhibit an excellent biocompatibility, allowing their use in the biomedical field, as dental, body prostheses, and tissue engineering [1].

Generally, ceramic parts are manufactured through conventional technologies, e.g. die pressing, gel casting, injection moulding, tape casting, etc. Into the required shapes from a mixture of powder with or without binders and other additives. Furthermore, several steps of machining and sintering to reach a higher densification and functionality are further needed. Nevertheless, these conventional forming techniques include several limitations; the production of highly complex geometries, which becomes unreachable due to the usual use of moulds, the high cost

and the long processing time. On the other hand, defects and undesirable shrinkages might also be generated in the ceramic parts and, in addition, due to their extreme hardness and brittleness, the machining of the ceramic components are highly challenging [2].

The introduction of additive manufacturing (AM) technologies, also known as 3D printing, into the manufacturing of ceramic components provides new possibilities for solving the challenges and limitations mentioned above. Following the ISO/ASTM 52900 definition (Reference ISO), AM is the process of joining materials to make parts from 3D model data, usually layer upon layer, as opposed to subtractive manufacturing and formative manufacturing methodologies. It enables the flexible preparation of highly complex and precise structures. Other advantages of AM include the productivity increase, as many objects can be built in a single run, and cost reduction respect to traditional manufacturing methods.

Within the different AM technologies, this paper is the first review focused specifically on powder bed selective laser processing (known as Selective Laser Sintering/Melting) of ceramics. This technique is a

---

powder bed-based method, which has similarities with other methods like binder jetting and powder bed fusion, for example. Topics around material/laser interactions, direct/indirect processing, feedstock, laser processing parameters are brought up to discussion. Furthermore, a more detailed description of the state of art for four specific ceramic materials is presented: Alumina, Silicon Carbide, Calcium Phosphate and Zirconia.

Consequently, the main objectives of the review are: to bring clarification on the discussed topics, sometimes matter of disagreements or misunderstandings among the research community working in the field; and to present the historical advancements and developments, state of art and future most-likely strategies to overcome the challenges for Powder Bed Selective Laser Processing (PBSLP) of Alumina, Silicon Carbide Calcium Phosphate and Zirconia.

## 2. History

Additive manufacturing began to be developed in the early 80's by several researches, using different strategies. However, in 1986 Carl R. Deckard, who was still an undergraduate student, filled the first patent [3], followed by two others later on [4,5], that defined what is known today as Selective Laser Sintering/Melting (SLS/M). Already in his first patent, Deckard wrote very clearly that this method was supposed to be suitable for different kinds of raw materials, in powder form: polymers, metals and ceramics.

In 1984, Deckard and his master's supervisor, Prof. Joe Beaman, started to work on a project designed by Deckard for the past few years. In his initial budget calculations, Deckard estimated a budget of around $ 30,000, considering a 100 W YAG laser. Three years later, the first academic machine, named "Betsy", allowed producing parts consistently enough to be presented to investors. Soon, a company named Nova Automation was licensed to develop SLS with an estimated budget of $300,000 and two years to raise it. Finally, in 1989, with some extra time/funding offered by the University of Austin Texas, Nova Automation had the necessary investment. Goodrich corp. Funded the idea with contracts up to $6 M. Other smaller grants were also obtained eventually. In 2001, after being sold once, the company was sold to 3D Systems, Inc., a company that developed Stereolithography and still produces SLS machines up to present days [6].

The first scientific publications involving SLS/M of ceramics were written right after the creation of the concept machine and method. Since 1992, several approaches started to be tested using ceramic materials, as ceramic/glasses mixtures [7] and polymer-coated ceramics [8], for

example. After these first publications on the field, the interest on developing SLS/M for ceramics is growing (Fig. 1). Considering alumina, Silicon Carbide, Calcium phosphates and Zirconia, this growth is similar. The large range of possible technical applications for these four materials attracts a consistent interest of the industry worldwide.

In 2015, Zocca et al. made an overview on Additive Manufacturing of ceramics, pointing the state of art at that time and the future expectations. A consistent description about different concepts on laser sintering was given by the authors [9]. In 2016, Ferrage et al. wrote a review on additive manufacturing of bioceramics, more specifically of alumina, zirconia and hydroxyapatite implementing Stereolithography (SLA) and SLS/M. The authors highlighted the need to optimize the process towards the raw materials, the AM parameters involved, post processing and mechanical properties. The global evaluation was that AM wasn't considered anymore a rapid prototyping technique exclusively [10]. In 2017, Hwa et al. reviewed the advances made in 3D printing of porous ceramics. Considering SLA, SLS/M, Fused Deposition Modeling (FDM) and Binder Jetting (called 3DP by the authors), the article put together information about several materials, including alumina, zirconia, hydroxyapatite (HA), Tricalcium-Phosphate (TCP), among others. The need of improving the raw materials in order to get better results is again brought to light, in this case, flowability and wettability are evidenced [11]. Also, in 2017, Sing et al. brought a discussion about direct laser sintering of silica and zirconia. The paper mainly discussed about layers deposition, laser interaction between the powder and the laser and parameters optimization. The authors observed critical behaviors on the relation between particle size and flowability and residual thermal stresses and melting [12]. In 2018, Hu and Cong reviewed AM of ceramics and ceramic reinforced metal matrix composites on laser deposition and some AM techniques (FDM, SLA, Inkjetting, Laminated Object Manufacturing, SLS/M). In 2019, Galante et al. provided information about AM of ceramics for dental applications, mainly discussing silica and silica-based systems, leucite, alumina and zirconia. The article compiled the state of art in each AM technique available for dental applications. The authors considered characteristics such as surface quality needed to be improved for a finished piece of high quality [13]. In 2020, Chen et al. compiled information about 3D printing of ceramics globally. The authors detailed recent results and brought the last available discussions about slurry-based, powder-based and solid-based techniques. It was also pointed out by these last authors that post-processing and parameters optimization are the great and next challenges [14].



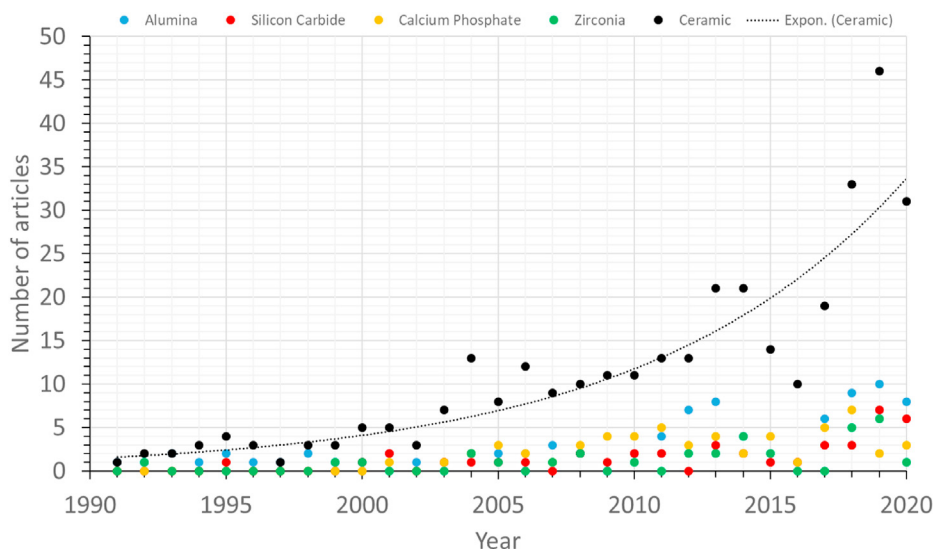**Fig. 1.** - Articles published between 1991 and August 2020, catalogued, listed and found in the webofknowledge.org database with the following keywords on article title: "selective laser sintering" or "SLS" or "selective laser melting" or "SLM" or "Powder bed fusion" or "PBF" or "laser sintering" or "laser melting" and the selected ceramic names or formula.

## 3. Powder bed selective laser processing (PBSLP)

The terms selective laser sintering and selective laser melting in additive manufacturing are not yet properly standardized. Every industry tends to maintain its own copyrighted names and moreover, these techniques are also applicable for polymers, plastics, metals, ceramics and non-metals. Due to these reasons, both terms are used interchangeably although the processes are different. During selective laser sintering, the particle coalescence of a powdered aggregate by diffusion is accomplished by firing at an elevated temperature and, in the other hand, during selective laser melting, the powder is transformed from solid phase into a liquid upon heating [15].

But, not all ceramics have a liquid phase, like for example silicon carbide, therefore, for materials that cannot be melted, we necessarily refer to selective laser sintering [16]. As the SLS/M process start from a powder and leads to a solid form by applying temperature both phenomenon, sintering and/or melting, can occur, but up to now studies have not evidenced which mechanisms occur for ceramic. Moreover, for example, if a mixture of polymer or another material with liquid phase and ceramic without liquid phase is used, under these circumstances, the use of selective laser melting and/or sintering does not seem to be clear either.

Both selective laser sintering and selective laser melting are techniques comprised within a process of additive manufacturing, Powder Bed Fusion (PBF), ISO/ASTM 52900 "Additive manufacturing — General principles — Terminology". Powder bed fusion methods use either a laser or electron beam to melt and fuse material powder together, following the same process than in the previous section [17]. However, again, due to the introduction of ceramics in the use of these techniques, as we have already mentioned, it is not always possible to achieve fusion and therefore the term is not used correctly either.

In conclusion, the current terms used in the literature show a limitation to correctly define the process in which a Powder Bed is Selectively Laser Processed and both sintering, melting and/or other phenomena could occur during the process. Consequently, to avoid misusing of the terms mentioned previously, a new term has been defined to refer this technique which fulfills the process criteria, Powder Bed Selective Laser Processing (PBSLP).

### 3.1. Process description

PBSLP is an additive manufacturing method that creates 3D solid pieces from a Computer Aided Design/Manufacturing (CAD/CAM) data by sintering/melting powdered materials layer by layer with the help of a laser [18]. [19] In a commercially available PBSLP equipment, mainly four sections are present whatever the company. The first essential part of a PBSLP machine is the laser. In today's market, PBSLP machines equipped with $CO_2$ ($\lambda$:10.6 $\mu$m) and Nd:YAG ($\lambda$:1.064 $\mu$m) can be found. Besides that, a few PBSLP machines are individualized by researcher groups which are equipped with both $CO_2$ and Nd:YAG laser for specific printing strategies like preheating. Other main parts of a PBSLP equipment are the powder storage space, the building platform, and the powder spreading tool. In a commonly accepted design, the build platform lowers by one layer and a scraper or a roller drum spreads an exact amount of powder from the powder stock side to the building platform side with a certain thickness. PBSLP machines equipped with a roller drum mostly has option of the compaction in order to increase the interaction between the granules in the deposited powder layer. Once the powder is dispersed in a thin layer on top of the building platform, the laser selectively sinters certain parts in the direction of the CAD/CAM design data. That layer by layer process continues through the entire piece. Any excess powder remaining after the printing session can be recovered after a proper sieving. Once all the printing parameters are individually optimized and set for a material and design, pieces with the same physical and chemical properties can be reproduced.

Certain limitations have to be faced during the PBSLP process of materials; in terms of laser-matter compatibility, building capacity and

thermal gradients etc. The most important criteria for a successful PBSLP processing is the compatibility between the laser used and the powder. For a proper sintering, the laser radiation energy should be absorbed by the powder. At the certain wavelength of the laser, each material shows a different energy absorption level [20]. In few cases, the amount of energy absorbed by the powder is not sufficient enough for compacting and forming a solid mass. In such a case, the laser absorption of a material can be enhanced by modifications like addition of an absorbent or processes like calcination. For example, Juste et al. used small amount of graphite as an absorbency enhancer for oxide ceramic powders and pieces with almost 90% density are obtained with a commercially available PBSLP machine [21]. Besides the laser absorption, another point in terms of laser used in the equipment is the spot size. Oxide ceramic powders such as $ZrO_2$, $Al_2O_3$ and $SiO_2$ interact differently at the $CO_2$ laser wavelength ($\lambda$:10.6 $\mu$m) than Nd:YAG laser wavelength ($\lambda$:1.064 $\mu$m), where the former has a substantial laser absorption, which is not observed in the latter. However, the amount of energy transferred to the powder bed still can be low due to the bigger spot size of the $CO_2$ laser which is resulting a decrease in the energy density. The relationship between the laser type, spot size and energy density should be studied carefully for each material.

As mentioned above, majority of the commercially available PBSLP machines are designed and used for polymers and metallic materials mostly. Lately, using PBSLP for the manufacturing of ceramic materials gained interest too. However, it has been quite challenging to obtain dense and mechanically stable ceramic pieces without any pre and post process. While metallic and polymer materials can tolerate the thermal gradients that occur between printed layers in PBSLP method, ceramics cannot. Equipment based modifications let a number of researchers to decrease these thermal gradients and increase the mechanical properties of the pieces. For example, preheating the building chamber and the powder bed up to just below the melting temperature narrow the thermal gap between the heating and the cooling [22]. Another method including a post-sintering/debinding process is also developed in order to shorten thermal gradients. In this method, the green body is obtained by only sintering the polymer powder in the powder blend including ceramic powder at very low temperatures. Then, the final density is obtained with an additional sintering/debinding step and the sacrificial polymer is mostly removed from the structure.

### 3.2. Direct/indirect powder bed selective laser processing

Powder Bed Selective Laser Processing of ceramics is classified in direct and indirect method. Some authors define that direct PBSLP is the method by which the ceramic powder is heated by a laser beam to bond particles as a result of solid state sintering or melting and, in contrast indirect PBSLP is the method by which the laser irradiation melts sacrificial organic polymer binder added to the ceramic powder, resulting in the bonding of the ceramic particles [23,24]. As a result, adapting the previous definitions, originally given for SLS and SLM, to our new term Powder Bed Selective Laser Processing of ceramics we redefine:

1. Indirect methods, make use of base material consisting of the ceramic phase mixed with a sacrificial polymer binder. The polymer binder has a lower melting point than the ceramic phase (if existing), and during laser scanning it melts and binds the ceramic particles together into a green part consisting of polymer and ceramic. Generally, post-processing techniques are used to remove the polymer binder and then to densify the ceramic via solid-state sintering or liquid-phase infiltration.
2. Direct methods, do not use a sacrificial binder. Instead, the ceramic material is directly sintered or melted into the desired geometry. In the case of direct laser sintering, post-processing techniques can be used to further densify the additively manufactured ceramics, for example by solid-state sintering or liquid-phase infiltration.

As we mentioned, the main difference between both techniques is the debinding process which is only present in the indirect method. Indirect PBSLP involves melting of a sacrificial (generally) organic binder phase to produce green parts. The green parts are subsequently debinded and sintered to produce ceramic parts. Direct PBSLP does not involve a sacrificial binder phase and the ceramic parts are produced by direct sintering or melting. Moreover, the presence of a binder in these techniques is not necessarily a condition to be considered as indirect. For example, Hon et al. mixed SiC particles with polyamide material, before laser sintering processing, with the polymer acting as the bonding system however, it is also an integral part of the final product rather than being removed in downstream processes and the process is considered as direct method [25].

### 3.3. Powder feedstock criteria

A successful powder bed in PBSLP technologies relies on a careful optimization of the powder properties (Fig. 2). Ensuring that a ceramic powder has good handling for PBSLP processing is still not possible only by analytical analysis, it is usually needed a trial and error investigation on the equipment as well [26]. Even if it is not possible to evaluate the handling of the powder with an exact accuracy there are different existing methods to evaluate their main features and deliver valuable information helping on the development of new or improved PBSLP powder feedstock [26].

Powder flow behaviour is known to have a direct impact on the quality and homogeneity of a spread powder bed and for hence, on the density of the powder and parts. Spierings [27] made an elaborate work collecting the comparisons that different authors made between existing powder flowability measurement techniques (static and dynamic) to determine the flow properties of powders (Table 1). Krantz [28] established that no single technique is suitable for a full characterization of a powder, it is required the use of different techniques to fully understand the flow properties of the powder and predict its behaviour under different process conditions. And hence, powder flow characterization technique should match the powder application in order to select the most appropriate characterization technique. AM processes use a ruler or a rotating cylinder as layer creation devices, where the powders have a high free surface and can be aerated to some degree depending on the speed of the device. Minimum limits on the flowability requirements will depend on the machine-specific differences, e.g. layer creation device (see Table 2).

Particle morphology (e.g. shape and surface) and size distribution of the powder have an important effect on final properties of the sintered artefact since they are directly related to the flowability and packing density of a powder bed. As a rule of thumb in different scientific fields, we can assume that for powders of narrow particle size distribution the most spherical and larger the particles, the better their flow behaviour [29–32]. The benefits of using multimodal powders as powder feedstock have been often exposed since the packing with a bimodal size distribution allows the smaller particles to fill the interstitial voids between the larger particles. A suitable size ratio between coarse and fine particles (over 1:10) and a weight fraction of large particles about 70% are the conditions showing maximum packing [33–35].

The laser is considered the most important part of a PBSLP device. Commercial devices can be equipped with either $CO_2$ lasers or Nd:YAG lasers (also called fibre lasers), being the last one the most common for industrial applications. One of the most important properties that will influence the laser-material interaction is the capacity of the powder to absorb the laser and transform the energy into heat to be sintered/melted. This is one of the issues that researchers have to face for the developing of new ceramic PBSLP powder feedstock. The wavelength of the laser should match with the maximum absorptivity of the powder to ensure the absorption of the energy. Some authors as Tolochko [36] and Ho [37] studied this matter with some important statements such as that the particle size distribution doesn't affect the laser absorptance of the material and that the use of composites can improve this property and hence, the interaction with the laser.

There have been some attempts of using reactive raw materials to fabricate 3D models of high-temperature structural materials like $Al_2O_3$ through an exothermic combustion reaction with low laser energy [38]. The main problem comes from connecting the layers of the piece to each other by having different reactivity. For this reason and because there are not many works on the use of this method in ceramic materials, this topic will not be covered in this review.

### 3.4. Process parameters and strategy

Many parameters belonging to the laser machine have an influence on the buildup process and, in the end, over the part's relative density. The
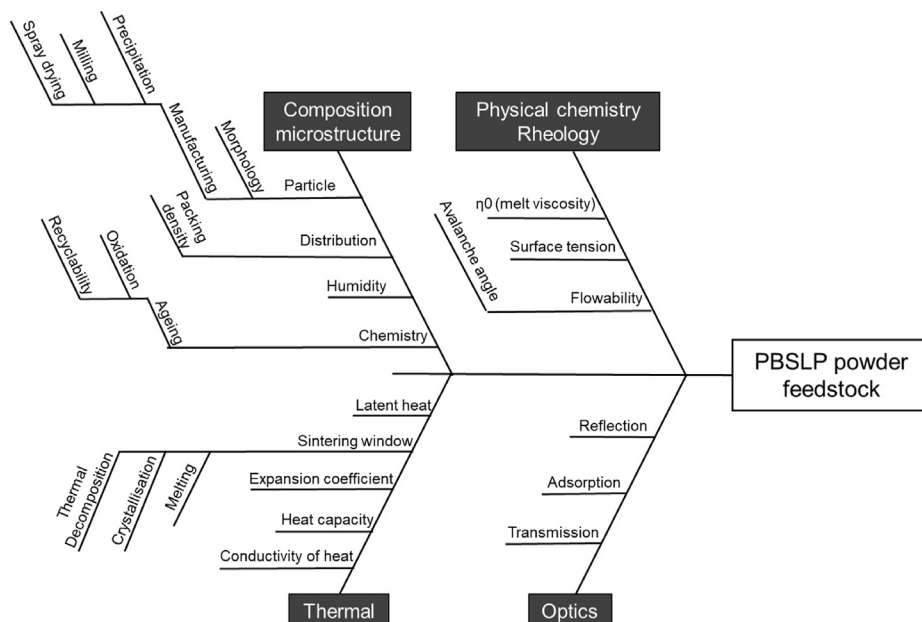


**Fig. 2.** Ishikawa diagram with influencing parameters for PBSLP powders (parameters listed in this articles [26,27]).

**Table 1**
Comparative of existing powder flowability measurement techniques [27].

| Powder flowability measurement technique | Details | Drawbacks |
|---|---|---|
| Ring shear cell tester (ASTM D6773) | - Industrial standard for measurement of powder flowability, compressive strength, compressibility, consolidation time, interal and wall friction, and bulk density. | - A compressive load is used during the assessment of powder, which does not suit well with the situation during AM process. |
| Hausner ratio HR (ASTM D7481-09) | - Common and widely used technique because of its simplicity.<br>- HR is defined as the ratio between tapped and bulk density. | - HR measurement differs of an AM process where thin powder layers are created and no compression or tapping is applied. HR is not considered to be ideal for application in AM.<br>- Powders often do not reach stable density after a certain number of tapping cycles, and a high dependency on the number of tapping has been elucidated. |
| Angle of repose/Hall flowmeter (ISO-4490/ASTM B213) | - Recommended by ASTM as the characterization method for metal powders for AM since the methodology is closer to the AM processing conditions than other techniques.<br>- Time required to discharge the powder and the angle formed for the powder pile are used as a measure for flowability. | - Operators filling method can influence the results.<br>- The diameter of the cone opening can be too small for some powders making difficult to quantitatively compare different powders.<br>- Not considered as best suited since stress state of the powder in the developed powder cone is still different to the AM process. |
| Avalanche test | - Nearer to PBSLP process that the other techniques.<br>- Good correlation with angle of repose method since similar stress states are induced to the powder.<br>- Avalanche angle, surface fractal, volume expansion rate and many more parameters can be measured. | - Not standardized yet |

user must manage it to have the best printed parts performance as possible by modifying those parameters (Fig. 2).

The power and the scanning speed are very related parameters since they define the amount of energy transferred in an area. While the power indicates the amount of energy transferred per second, the speed will control the time spent in the same area. An equilibrium between both has to be reached to avoid the formation of pores, either by too much or insufficient energy. For the same scanning strategy, the scanning speed, together with the hatching distance and the layer thickness will control the build rate. The build rate coefficient is the volume of material produced per hour, normally expressed in cm$^3$/h and is used to compare processes productivity:

$$B = h * t * v \tag{1}$$

where $B$ is the build rate coefficient (mm$^3$/s), $h$ the hatching distance (mm), $t$ the layer thickness (mm), and $v$ is the scanning speed (mm/s).

A higher scanning speed will lead to higher productivity, therefore, it is important to try to increase it. Always taking into account that too high speed will produce poor sintering or melting of the part resulting in the formation of pores. Alternatively, excessively slow speed can evaporate the material forming pores and imperfections as well.

The layer height or layer thickness is the distance between layers and it also has an impact on the build rate. A lower number of layer spread means that the recoater will be used fewer times having a big impact on the processing time. Additionally, the higher the layer thickness is, the lower the resolution of the part will be. In addition, if this distance is too large, it can lead in a poor attachment between layers and the braking of the part. For all this, the layer height must be the highest as possible, but shorter enough to ensure the attachment between layers and avoid possible breaks.

The hatching distance refers to the distance between centres of adjacent laser beam tracks. This parameter affects the build rate as previously explained. It is necessary to find the correct distance between tracks to avoid zones with no or not enough interaction with the laser beam leading to unreacted powder, even if there is some powder is stroke by two different laser tracks, causing an overlap. A distance to obtain a good quality part but at the same time optimizing the build rate of the process should be pursued.

During PBSLP process it is possible to shift the laser beam focus, or "defocus", by displacing the building platform in the z-axis to increase the laser spot size [39]. The diameter of the spot during the PBSLP process can influence the energy transmitted and the area affected by the powder bed. It can also originate different microstructure to the piece

due mainly to a different cooling rate. Additionally, some PBSLP machines are equipped with a rotating cylinder as part of the recoating device been able to perform a controlled compression of the powder bed after its spreading. The compression would increase the packing density of the powder bed and hence have a direct influence on the final density and quality of the printed parts. The chemical species present in the chamber atmosphere during PBSLP can induce different effects on the material being irradiated since high temperatures are reached. While an inert atmosphere can avoid any chemical reaction (i.e. combustion, phase transition …) from taking place during the process, atmospheric "air" could favor it. It is the work of the user to find the best conditions to print the material in question.

Even if there are many parameters involved, most of the current research on the process optimization have only in consideration the energy density ($E_d$) or energy input in a defined volume that can be calculated through:

$$E_d = \frac{P_{laser}}{v_{scan} . h_{space} . t_{layer}} \left[ \frac{J}{mm^3} \right] \tag{2}$$

where $E_d$ is the energy density or energy input in J/mm$^3$, $P_{laser}$ is the laser power (J/s), $v_{scan}$ the scanning speed (mm/s), $h_{space}$ the hatch distance (mm), and $t_{layer}$ is the powder layer thickness (mm). This parameter should be considered an approximation since lot more aspects affect the real energy transferred to the powder bed such as the direction of gas flow, laser diameter, scan strategy, offset at the surface of the melt and so on [40,41]. Although recent studies have started to evaluate the effect of the scan strategy during the fabrication process [42,43]. The use of the diameter of the laser beam ($d_{spot}$) in equation 3 instead of $h_{space}$ can be found in some studies. Even if the basic concept is the same, both parameters should be coordinated to control a certain overlap ratio [40].

Fig. 3 illustrates the different parameters that compose the $E_d$ for a better understanding. Thus, $E_d$ is the energy that the laser beam transfers per unit volume of powder bed and serves as a broad guideline for parameter selection. However, it is a thermodynamic quantity, and $E_d$ does not include the kinetics of the irradiated material physics missing a correct understanding of the mass and heat transfer between the laser track and the surrounding material such as spattering of irradiated material. A careful approach is recommended when comparing results from experiments done under different conditions even to the same material and when testing new parameters [44].

The scanning strategy is the pattern that the laser beam follows to irradiate the selected region of the powder bed (see Fig. 4). It controls the energy density distribution during the process and as explained above, it

**Table 2**

Summary of the process conditions and properties of the CaP sintered scaffolds by the PBSLP process. PM= Powder mixture *Values will be given when possible. PS: Particle size, HDPE: high-density polyethylene, PHBV: poly (hydroxybutyrate–co-hydroxyvalerate), CHA: carbonated hydroxyapatite, PLLA: poly (ʟ-lactic acid), PCL: poly-e-caprolactone, EP: Epoxy resin.

| Ref. | Year | Powder feedstock | Laser & strategy | Post-processing | Properties of processed parts* |
|------|------|------------------|------------------|-----------------|-------------------------------|
| Hao et al. [59] | 2007 | HA (20%)/HDPE 0 < PS < 105 μm & 105 μm < PS | $CO_2$ 3.6–6.0 W Scan speed 3.6 m/s Line spacing 63 μm Layer thickness 150 μm Powder bed T: 128 °C | No post-processing | Porosity: 45–55% Wettability: 60–140 deg. |
| Xiao et al. [60] | 2008 | PM1: Apatite/Wollastonite (PS: 45–90 μm) + 5% acrylic binder PM2: Apatite/Wollastonite (64% PS 45–90 μm 21% PS 0–45 μm) + 15% acrylic binder | $CO_2$ 250W Spot size 0.6/1.1 mm Layer thick. 125 μm Line spacing (spot size/2) (Indirect) | Heat treatment process + infiltration of CaP glass | Bend strength: PM1 35 MPa PM2 70 MPa PM2 with CaP glass infiltrated 100 MPa Porosity: 40% |
| Duan et al. [61] | 2010 | PM1: PHBV (d50: 53.18 μm) PM2: nanoCaP 15%/PHBV (d50: 46.34 μm) PM3: PLLA (d50: 40.03 μm) PM4: nanoCHA 10%/PLLA (d50: 39.78 μm) | $CO_2$ laser 13–15W Spot size 457 μm Scan speed 1257 mm/s Line spacing 100–150 μm Layer thick. 100–150 μm Part bed T: 35–45 °C | No post-processing | Porosity: 62.6–68.5% Compressive strength (dry scaffolds): 0.47–0.62 MPa Strength modulus (dry scaffolds): 5–6.5 MPa |
| Cruz [54] | 2010 | HA 60% (d50: 111 μm)/PLLA (d50: 163 μm) | $CO_2$ laser 5–7.5 W Scan speed 200–300 mm/s Line spacing 100–150 μm Energy density 2.66–8.96 cal/cm2 | No post-processing | Compressive strength: 2.4–4.6 MPa Bend strength: 1.6–4 MPa Density: 0.78–1.1 g/cm3 |
| Eosoly et al. [51] | 2010 | HA 30% (d50: 38 μm)/PCL (d50: 125 μm) | $CO_2$ laser fill 8.32–11.68 W (outline laser 3.32–6.68 W) Spot size: 410 μm Line spacing 100–200 μm Layer thickness 150 μm Part bed T: 38 °C | No post-processing | Density: 0.33 g/cm3 Compressive strength: 1–2 MPa |
| Shuai et al. [58] | 2013 | Nano-HA (d50: 0.06–0.1 μm) 0%/10%/30%/50%/70%100%/β-TCP (d50: 0.1–0.3 μm) | $CO_2$ laser 12 W Spot size 800 μm Scan speed 100 mm/min Layer thick. 200 μm | No post-processing | For HA 70%/β-TCP scaffold: Porosity: 61% Fracture toughness: 1.33 MPa.m$^{1/2}$ Compressive strength: 18.36 MPa Higher bone-forming ability and balanced biological stability and dissolution rate. |
| Xia et al. [52] | 2013 | PM1: 0%-5%–10% needle-like nano-HA (150 nm long, 20 nm wide)/PCL PM2: needle-like nano-HA 5%/10%/PCL | $CO_2$ laser fill 4.5 W (outline laser 3 W) Spot size 150 μm Internal scan speed 1.25 m/s Peripheral scan speed 0.55 m/s Support scan speed 1.33 m/s Layer thick. 150 μm | No post-processing | Porosity: 70.31–78.54% Compressive strength: 1.38–3.17 MPa More effective osteogenesis than pure PCL scaffolds |
| Colin et al. [48] | 2014 | Examples 1 & 2 respectively: PM1: HA 95–99% (d50: 5–25 μm)/Absorption additive (Carbon) PM2: TCP (d50: 5–25 μm)/Absorption additive (SiC) (d50: 1 nm–100 μm) | PM1: Nd: YAG laser 40 W Scan speed 100 mm/s Line spacing 200 μm PM2: Nd: YAG laser 100 W at 10% 10% defocused Scan speed 20 mm/s | PM1: Thermal treatment to improve mechanical strength at 1100°C-2h PM2: Thermal treatment at 300–1200 °C for 10 min to 5 h. | |
| Ferrage et al. [62] | 2018 | Pure HA (d50: 75 μm) | $CO_2$ laser 220W Spot size 200 μm Scan speed 100 mm/s Line spacing 800 μm Layer thick. 100 μm | No post-processing | Decomposition of HA into TTCP and CaO observed. Density: 3,0691 (helium pycnometer) |
| Zeng et al. [55] | 2020 | EP (d50: 20 μm) 35%/40%/45%/50% in wt./BCP (70/30 ratio of HA and TCP) (d50: 80 μm) | $CO_2$ laser 1.8W Spot size 200 μm Scan speed 200 mm/s Line spacing 150 μm Layer thick. 100 μm | Sintering of green part at 1100 °C for 4 h for binder removal. (Indirect method) | Scaffold with EP and BCP 50/50 ratio showed superior mechanical properties: Compressive strength: 113.25 KPa Porosity: 80.8% Elastic modulus: 4.38 MPa This scaffold showed the most outstanding bioproperties in terms of osteogenic differentiation, ALP staining, ALP activity, and OCN immunocytochemistry. |
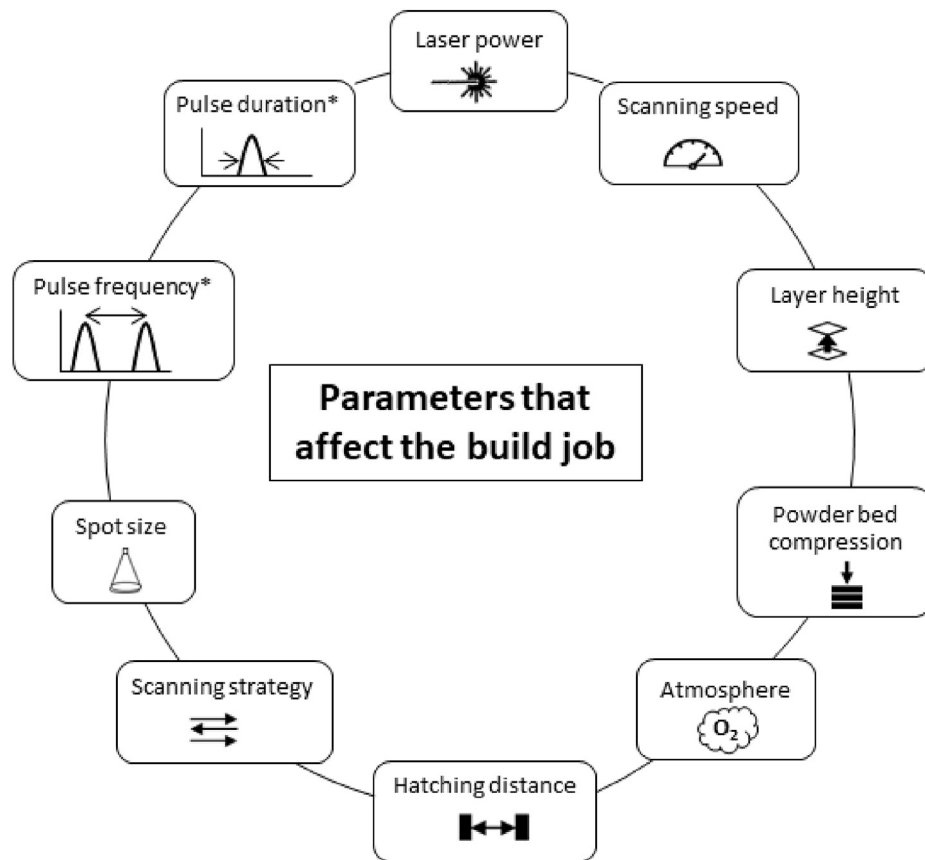
Fig. 3. Example of process parameters that can be programmed. *Belonging to pulsed lasers.

has an important effect on the final structural properties of the printed parts. Fig. 5 illustrates some examples of scanning strategies used in PBSLP. It is important to find the scanning strategy in which an optimal energy density distribution occurs for each material thus avoiding adverse effects like decomposition, thermal cracks, and so on.

## 4. PBSLP of calcium phosphate, silicon carbide, zirconia, alumina, and their composites

### 4.1. Calcium phosphate

Calcium phosphate (CaP) bioceramics are widely used in medical applications in many different ways such as coatings, paste, scaffolds, and cements. The use of a PBSLP process could allow the manufacturing of patient-matched tissue engineering scaffolds with controlled inter-connected porous network and shapes made of CaP. With the present document, we wanted to explain the more recent studies focused on the two phases forming biphasic calcium phosphate (BCP) since they are the CaP phases most used to produce scaffolds through PBSLP process. Hydroxyapatite (HA) and β-Tricalcium phosphate (β-TCP) form BCP at different ratios to be used as bone-substitution bioceramics.

In the case of bone graft, the main role of a scaffold would be to provide a framework for the regeneration of new bone tissue, soft tissue, vascular-, and other metabolic-components. CaP materials gather several critical properties needed for the correct performance of a bone graft material. For example, they can promote the formation of new biological tissue reducing the response from the immune system of the organism or tissue through its osteoconductivity (or osteoinductivity) and biocompatibility. Resorption is the term used to describe the absorption of a bioceramic in the body, either by dissolution or by cells (such as macrophages and osteoclasts). The desired resorbability rate is the rate comparable to the formation of bone tissue (between a few months and a few years), in the case of CaP, it may take 3–36 months to be replaced by bone. This property depends on the phase content of the CaP, crystallinity, lattice defects, particle size, and porosity. Some CaP phases like TCP may resorb fast and replace the coating or cement with bone. Other CaP phases like HA have a low resorption rate but they are osteoconductive materials acting as scaffold promoting the formation of new bone [45].

The use of CaP bioceramics in the bone replacement field requires also good mechanical properties. This is due to the high average load that the parts undergo during their lifetime. CaPs are brittle (primary ionic bonds) with relatively low tensile stress (6–10 MPa) and low impact resistance because of their porosity acting as preferred initiation sites for crack propagation. However, their compressive strength is higher than that of normal bone. For that reason, CaPs are more used in non-load bearing implants [45].

One important advantage is the chemical resistance of the ceramic implants respect to metal implants. The human body is a very harsh environment for metals since it contains water, salt, dissolved oxygen, bacteria, proteins, and various ions such as chloride and hydroxide. HA coatings have demonstrated to have excellent chemical resistance; that is why they are widely used to coat base metals to ensure biocompatibility of the ceramic on the metal surface. Furthermore, another benefit of HA is their dielectric properties (piezoelectricity) because electromagnetic fields have been shown to accelerate healing in bone fractures [46,47].

Some solutions have been conceived to compensate for the low absorption of the laser by CaP powders during PBSLP. An increase of the energy density delivered during the process is usually performed by intensifying the power of the laser, reducing its speed, and/or by using other sources of energy. But it leads to a loss of productivity, poor final quality of the scaffolds, and cost-ineffectiveness. A method to deal with the low absorptivity of CaP materials of Nd:YAG laser and perform the bonding of CaP particles and the subsequent manufacturing of
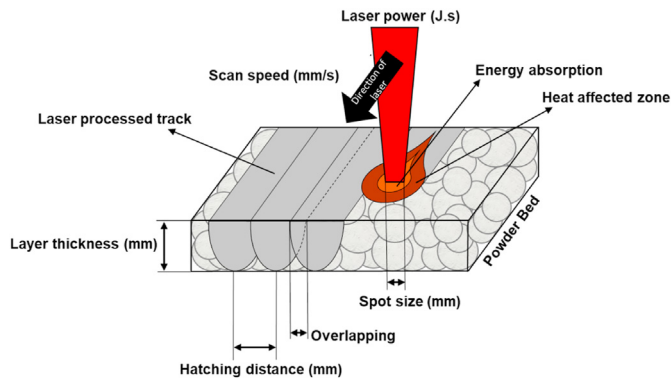
**Fig. 4.** Scheme of variable parameters involved during the PBSLP process and from which the $E_d$ can be calculated.

biomedical devices is disclosed by Colin et al. [48] It consist on the mixing of the ceramic substrate with an absorption additive before the PBSLP process. In this method, the ceramic powder constitutes the predominant portion by weight of particles together with a dispersed absorption additive. This additive has a higher specific absorptivity at the wavelength of the laser used than the ceramic components and it can be biocompatible, biodegradable, soluble and/or heat degradable. It is used for transferring the radiant energy of the laser into thermal energy to melt/sinter the ceramic material in the mixture. This method is considered a direct PBSLP process.

The decomposition due to high temperature and the subsequent adverse effect on the mechanical properties is another important challenge that researchers have to face when printing CaP materials through PBSLP process. It has been already studied in plasma spray coating processes that the sintering temperature usually triggers the phase transformation of HA or β-TCP scaffolds into other CaP phases. Phases such as tetracalcium phosphate (TTCP), α-TCP, and/or calcium oxide (CaO) can be produced before melting, which can influence densification process. Porosity and grain size changes produced by the phase transition were found to play an important role in the mechanical performance of sintered HA. The decomposition of HA is a process of continuous reactions depending on the obtaining conditions. Ramesh et al. [49] performed a study of the sintering properties of HA powders prepared by different methods concluding that the HA powder prepared via the wet precipitation method shows better thermal stability, translated in less phase transformation and superior better mechanical properties. However, the usual mechanical behaviour limitations of CaP materials, in terms of brittleness, poor fatigue resistance, low tensile strength, and low fracture toughness value preclude HA from use in load-bearing situations.

To deal with the drawbacks previously mentioned, numerous works using CaP powders as part of composite materials to produce scaffold through the PBSLP technique have been reported [50–53].

In one direct method approach the CaP powder is used as a filler in a mixture together with a polymer matrix and provides bioactive properties

and higher strength to the scaffold [51,52,54]. Poly-ϵ-caprolactone, polyethylene (PE), high-density polyethylene (HDPE), and poly (ʟ-lactic acid) (PLLA) are the most often used polymers in such composite materials. Due to the lower temperature needed to melt and bond the polymer particles, the ceramic phase transformation is avoided. Although the time of implantation can have some adverse effects on polymeric materials losing some of their properties. These polymers are not removed after the PBSLP process, being the main part of the final scaffold used in the application. For this reason, these works are part of the direct PBSLP category. Even if the application is currently limited to the field of the filling of bone defects this method results in the production of promising improved bioactive scaffold with higher strengths and stiffness than the unfilled polymer (Fig. 6).

A different approach is an indirect method, consisting of the use of polymers as a binder together with calcium phosphate powders as the main matrix in the composite. The organic polymer is melted during the PBSLP process to obtain a green part, afterward, the green part is sintered removing completely the binder and producing the final porous ceramic part. Then the final part will be composed of pure ceramic. Recently, Zeng et al. [55] achieved the production of microporous BCP scaffolds by low-temperature PBSLP keeping the physicochemical properties of BCP and improving the mechanical strength, porosity, and bioproperties. In this case, epoxy resin was used as a sacrificial organic polymer and was completely decomposed and removed by a posterior sintering process.

Shuai et al. [56–58] attained the fabrication of pure CaP ceramic scaffolds of nano-HA and BCP in different proportions using a homemade PBSLP system equipped with a $CO_2$ laser. Although the presence of CaP secondary phases due to the phase transformation during the sintering process was confirmed by XRD analysis. Nano-HA powder used had a needle-like or irregular shape and β-TCP powders were mostly spherical with also a nanometric size. A ratio of TCP/HA (30/70) was found to exhibits the most outstanding resorption properties. Fig. 6 (b) shows the porous BCP scaffold with 3D orthogonal porous square channels with 13 mm in width, 7 mm in height, spaced by 2 mm, and a porosity of 61% measured with the Archimedes method.

To summarize, the main advantages of using PBSLP technique for the fabrication of CaP pieces lie in the flexibility to produce complex and well-controlled porous scaffolds with no need for supports or post-processing. There are some requirements that the powder feedstock has to fulfil to obtain good results, and as we observed, different approaches have been developed within the last years. Diverse powder feedstocks have been developed combining CaP materials between them and with a wide variety of additives and/or polymers/bioglasses to surpass the issues of CaP materials in PBSLP. There is still a need for research on the improvement of the mechanical properties and the resolution of the scaffolds to ensure their correct performance in bone tissue engineering applications. Their brittleness still limits their clinical application especially for load-bearing implants. Although they showed promising results in terms of bioactive properties. Even if the tendency is to start modifying the initial powder feedstock, the improvement of PBSLP devices with a better design and a range of parameters adapted for better processing of ceramic materials will be crucial for their future in PBSLP processes.
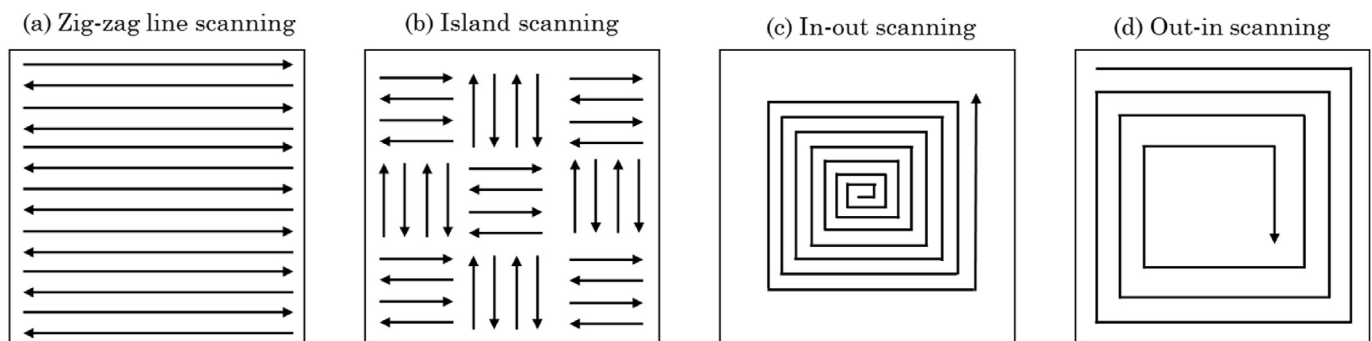


**Fig. 5.** Examples of different scan strategies that the laser can follows during PBSLP.
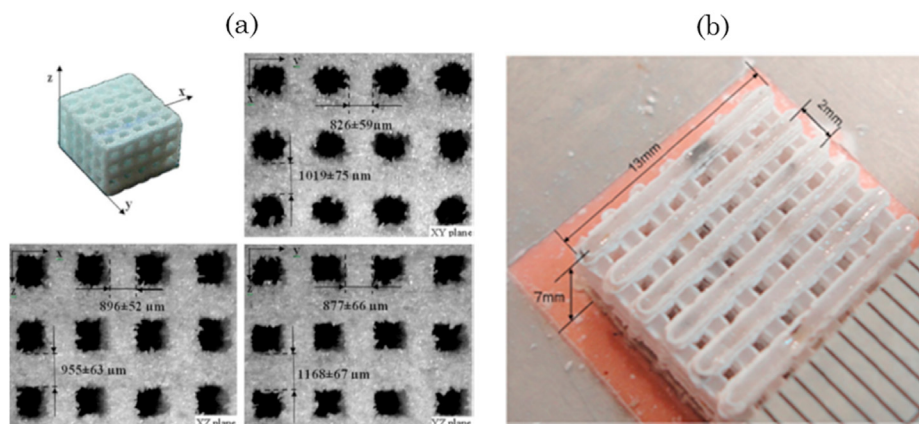
**Fig. 6.** Sintered scaffolds made by PBSLP process using different calcium phosphate materials and composites. (a) Nano-HA/poly-e-caprolactone [51] and (b) BCP [58].

## 4.2. Silicon carbide

Because of its excellent properties such as its high mechanical stiffness, low density, wide bandgap, low coefficient of expansion, high thermal stability, and resistance to corrosive environments, Silicon carbide (SiC) is an enabling technology for many applications. Among these applications are high-power microwave devices for commercial and military systems; electronic devices (LED's, MOSFET's); high temperature electronics/optics for automotive, aerospace (space telescope mirrors), laser processes mirrors and well-logging; rugged MEMSs (micro-electro-mechanical sensor) devices for hostile environments; gas and chemical sensors for internal combustion engines, furnaces, and boilers; and solar-blind UV photodetectors [63]. To manufacture some complex SiC parts, regular industrial processes have been successfully developed since the 90's [64]. However, for some specific applications, due to the enormous advantages of manufacturing complex structural ceramics, additive manufacturing (AM) has been extensively studied since the component design could be improved by this emerging technology. As one of additive manufacturing methods, PBSLP has been expected to fabricate complicated shape SiC components in recent years. However, silicon carbide ceramic parts prepared selective laser sintering still exhibit some fatal defects, including low densities and poor mechanical properties. In this respect, indirect selective laser sintering can be adopted to form silicon carbide ceramic components by sintering polymer binders in a composite powder [65,66].

SiC does not have a melt phase under normal atmospheric circumstances but instead decomposes at temperatures in excess of 2545 °C into liquid Si and solid C [23]. In consequence, pure selective laser melting of silicon carbide cannot be done. To solve this problem, different solutions have been adapted depending on whether a direct or indirect SLS strategy is used.

The first research to achieve direct PBSLP of SiC was in 1993 by scanning silicon powder in an acetylene ($C_2H_2$) chamber where silicon carbide could be formed by the reaction of Si with the carbon in the atmosphere. However very porous ceramic parts with high SiC content were obtained [67]. To increase the density by direct PBSLP processing of the final SiC part, Hon et al., in 2003 manufactured SiC/Polyamide composites by blending 50 vol% polyamide with 50 wt% SiC for direct SLS processing. After the PBSLP process, the polymer is also an integral part of the final product rather than being removed in downstream processes. Nevertheless, the finals parts had poor mechanical properties [25]. In these terms, Löschau et al. used silicon infiltration in complex pure SiC parts where their mechanical and thermal properties can be improved and controlled via Si content [68]. Moreover, during this period, different authors developed a micro laser sintering to fabricate SiC ceramics [69,70] by blending Si–SiC powder beds with a q-switched laser. These techniques contributed to the development of current

research work. As one example, Meyers. et al. [71,72] laser sintered a powder mixture of silicon carbide (SiC) and silicon (Si) powders where the Si melts and re-solidifies to bind the primary SiC particles. Afterward, these Si–SiC preforms were impregnated with a phenolic resin, which was pyrolysed yielding porous carbon and transformed into secondary reaction formed SiC when the preforms were infiltrated with molten silicon in the final step. This resulted in fully dense reaction bonded silicon carbide parts with up to 84 vol% SiC.

In the terms of indirect PBSLP, first research was carried out at the University of Texas in Austin in 1993, where indirect PBSLP of reaction bonded silicon carbide was firstly investigated [8]. Since then, we can observe different combinations of powder and different binders that were used in order to increase the density and properties of the additive manufactured SiC parts (Table 3). Apart from the use of binders, another solution to reduce the porosity of the final parts was the use of the infiltration of a precursor carbon resin (phenolic resin) in the porous green part structure, then carbonized (polymer infiltration pyrolysis) and finally infiltrated with molten silicon (reaction sintering) to build SiSiC (Reaction bonded silicon carbide) which improved the properties of complex shaped Si/SiC prototypes [73]. Moreover, in recent years, different post-treatments were investigated as another method to reduce the porosity of the additive manufactured parts. The combination of Cold Isostatic Pressing (CIP), as a post-treatment, after the PBSLP process with the combination of polymer infiltration pyrolysis (PIP) and reaction sintering (RS) in this strict order, built SiC based 3D parts that, compared with the best flexural strength at room temperature in literature, increased the peak value of flexural strength by 55% [74] and 94% of relative density [65].

To summarize, on the one hand, indirect PBSLP based approaches require a high amount of polymer binder and yield ceramics with a substantial amount of porosity. This method induces a substantial amount of shrinkage between the laser sintered and the post-sintered final ceramic. Moreover, debinding has to be done carefully in order to avoid crack formation due to excessive out-gassing. In these terms, indirect PBSLP can therefore not be considered as a net-shaping technique, since dimensional changes occur during processing. On the other hand, direct PBSLP methods do not induce shrinkage and are generally less time-consuming than indirect methods. However, SiC is notoriously difficult to process directly since the lack of melt phase under normal circumstances. Although the use of silicone powder allows manufacturing parts based on silicon carbide, it is still a challenge to manufacture full dense parts with a SiC pure composition (see Fig. 7).

## 4.3. Zirconia

Zirconia ($ZrO_2$) is the crystalline dioxide form of zirconium which is commonly used in various industries such as electronics and biomedical

**Table 3**
Summary of the process conditions and properties of the SiC manufactured by the PBSLP process. *Values will be given when possible.

| Reference | Year | Powder feedstock | Laser and strategy | Post-treatments | Properties of processed parts * |
|---|---|---|---|---|---|
| Vailt et al. [75] | 1993 | Polymer (polmetgylmethacrylate) encapsulated silicon carbide | Indirect SLS (CO2)<br>Laser Power: 6–16 W<br>Scan speed: 50–100 ips (1270–2540 mm/s)<br>Beam Spacing: 2–5 mils (0.05–0.13 mm)<br>Layer Thickness: 4,5 mil (0.11 mm) | No post-processing | 46%–50% of relative density |
| Birmingham et al. [67] | 1993 | Silicon powder + C2H2 precursor gas | Direct SLS (CO2)<br>Laser Power: 1.8–2.8 W<br>Scan speed: 500 $\mu$m/s<br>Hatching Distance: 50 $\mu$m | No post-processing | (Not determined) |
| Nelson et al. [8] | 1995 | 25 vol % PMMA-coated SiC | Indirect SLS (CO2)<br>Laser Power: 6–16 W<br>Scan speed: 50–100 in./s (1270–2540 mm/s)<br>Hatching Distance: 0.002–0.005 in. (0.050–0.127 mm)<br>Layer Thickness: 0.0045 in. (0,1143 mm) | No post-processing | 57% relative density<br>Green strength = 205.8 psi |
| Stierlen et al. [73] | 1995 | SiC + reactive polymer binder | Indirect SLS (CO2) | Precursor resin infiltration + pyrolysis + Molten silicon infiltration | (Not determined) |
| Löschau et al. [68] | 2000 | SiC | Direct SLS (CO₂)<br>Laser power: 45–52 W<br>Scan speed: 200–300 mm/s<br>Layer Thickness: 50 $\mu$m<br>Atmosphere: Argon/air mixture | Liquid Si Infiltration | Mass density: 2.65 g/cm$^3$<br>Bending strength: 195 MPa<br>Young's modulus: 225 GPa<br>Thermal expansion coefficient: $40 \cdot 10^{-7}$ K$^{-1}$<br>Thermal conductivity: 70 W/mK |
| Hon et al. [25] | 2003 | 50 vol% polyamide + 50 wt% SiC | Direct SLS (CO2)<br>Laser Power: 4–8 W<br>Scan speed: 1000–1250 mm/s<br>Hatching Distance: 0.15–.0.2 mm<br>Layer Thickness: 0.1–0.125 m | No post-processing | Tensile strength = 46 MPa<br>Young modulus = 2200 MPa |
| Evans et al. [76,77] | 2005 | SiC + char-yielding polymer | Indirect SLS (CO2) | Precursor resin infiltration + pyrolysis + Molten Si infiltration | 95% of relative density |
| Stevinson et al. [16, 78] | 2008 | SiC + phenolic resin | Indirect SLS (CO2)<br>Laser Power: 10 W<br>Scan speed: 1.3 m/s<br>Hatching Distance: 100 $\mu$ m<br>Layer Thickness: 75 $\mu$ m<br>Atmosphere: Nitrogen<br>Bed Temperature: 75 °C | Precursor resin infiltration + pyrolysis + Molten Si infiltration | Full dense bodies |
| Xiong at al [79]. | 2013 | nylon 6 (15 wt%) + NH4 H2 PO4 (5 wt%) + SiC (80 wt%) | Indirect SLS (CO2)<br>Laser Power: 15 W<br>Scan speed: 1200 mm/s<br>Layer Thickness: 0.1 mm<br>Bed Temperature: 175 °C | Thermal treatment at 700 °C for 1 h | linear shrinkage up to 98.89%<br>Tensile strength: 3.56 MPa<br>Bend strength: 1.75 MPa |
| Meyers et al. [71, 72] | 2018 | Silicon 40%. vol.+ Silicon carbide powder 60% vol. | SLS (Fiber Laser)<br>Laser Power: 12–21 W<br>Scan speed: 50–500 mm/s<br>Hatching Distance: 77 $\mu$ m<br>Layer Thickness: 30 $\mu$ m | Phenolic resin infiltration + Curing + Pyrolysis + Liquid Si Infiltration | Full dense body with Vickers hardness of 2045 HV, an electrical conductivity of 5.3 × 103 S/m, a Young's modulus of 285 GPa and a 4-point bending strength of 162 MPa |
| Jin et al. [66] | 2018 | SiC + epoxy resin (3% wt.) | Indirect SLS | Cold isostatic pressing + polymer infiltration pyrolysis | Porosity = 22.03%<br>Density = 2.48 g/cm3 |
| Liu et al. [65] | 2018 | Formaldehyde resin (18% wt.) + SiC | Indirect SLS<br>Laser Power: 6–10 W<br>Scan speed: 1700–2300 mm/s<br>Hatching Distance: 0.1–0.2 mm;<br>Layer Thickness: 0.1–0.25 mm | Cold isostatic pressing + Reaction Sintering | Bending strength = 292–348 MPa density = 2.94–2.98 g/cm3 |
| Song et al. [74] | 2019 | SiC + spheroidal-graphite + coarse silicon particles + Epoxy resin + Dicyandiamide | Indirect SLS (CO2)<br>Laser Power: 18 W<br>Scan speed: 3500 mm/s<br>Layer Thickness: 0.1 mm | No post-processing | Peak value of flexural strength increased by 55% |
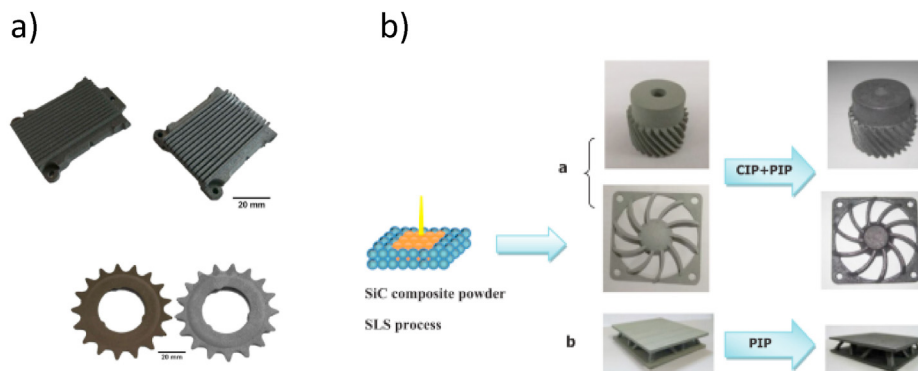
**Fig. 7.** a) Direct laser sintering of reaction bonded silicon carbide with low residual silicon content [70] b) SiC/SiC composites prepared by SLS combined with Polymer Infiltration Pyrolysis (PIP) and Cold Isostatic Pressing (CIP) [66]. (For interpretation of the references to color in this figure legend, the reader is referred to the Web version of this article.)

devices [80]. This polymorphic material shows three different phases depending on temperature at ambient pressure, thus, it cannot be used as itself in many applications [81]. Between the room temperature and 1170 °C, the monoclinic phase (m, space group P2$_1$/c) occurs. The tetragonal phase (t, P4$_2$/*nmc*) presents from 1170 °C up to 2370 °C, and above that temperature the cubic phase (c, Fm3m) can be found up to the melting temperature (2690 °C) [82]. During heating and cooling these phases are reversible which results in an increase or a decrease in volume. This change in volume (0.5% during c → t transition and 4% during t → m transformation) which can result in catastrophic failure in structure has limited the use of zirconia for a long time. Thus, failures due to the volume expansion and reduction can be prevented by stabilizing of pure zirconia in desired phases. From that day on, the potential of fully-partially stabilization of zirconia was discovered and used in many areas due to its superior properties such as chemical inertness, biocompatibility, extremely high strength, and fracture toughness. Garvie et al. showed that the most useful mechanical properties can be improved by obtaining a multi-phase structure which is known as partially stabilized zirconia (PSZ) [83]. They were able to disperse tetragonal grains in a cubic matrix by addition of calcium oxide. This tetragonal metastable phase rich structure can transform to the monoclinic phase that ends up with an increase in the fracture toughness and strength of the material. Zirconia was fully stabilized in cubic phase by adding 3.5 wt % amount of calcium oxide by Ruff et al. [84]. Nowadays, the stabilization of pure zirconia can be done with various oxides such as magnesium oxide (MgO), yttria (Y$_2$O$_3$), cerium (IV) oxide (CeO$_2$), or lanthanum oxide (La$_2$O$_3$). Among all, yttria stabilized zirconia (YSZ or TZP) is the most commonly used one. Lately, it is preferred to name a Y-TZP composition

with its yttria molar ratio (such as 3YSZ or 3Y-TZP for 3 mol% yttria stabilized zirconia) in order to avoid misunderstandings.

Yttria stabilized zirconia has various application areas due to its great and unique properties. YSZ is commonly used as electrolyte (mostly cubic phased 8YSZ) in manufacturing of solid oxide fuel cells (SOFC) and as coatings for thermal barrier applications. As a bulk material, YSZ is prevalently used in biomedical applications such as orthopedic implants and dental prosthesis [85]. While other novel oxide ceramics are being studied as an alternative to YSZ, it is still commonly used for its greater fracture toughness. Its superior corrosion and wear resistance, and also its good biocompatibility make YSZ a good candidate for biomedical applications. Especially for joint (hip, knee etc.) and for dental implantology, yttria stabilized zirconia is commonly used. Biomedical grade zirconia is mostly stabilized with 3 mol% yttria in order to maintain the desired mechanical properties of the tetragonal phase at room temperature. Its off-white color makes YSZ favorable for dental implantology in terms of esthetics. 3Y-TZP was used to manufacture femoral heads for total hip arthroplasty in the late 90s. These orthopedic devices were used in patients by 2001, until continuous femoral head fractures were reported. Although there were not mechanical and thermal stress, the catastrophic t → m transformation was triggered. Studies showed that, a wet environment can also cause the low thermal degradation (LTD) or ageing by filling the oxygen vacancies with water radicals. Thus, various studies are carried out in order to improve LTD resistance of zirconia by stabilizing it with other oxides such as CeO [86]. Composites consisting of zirconia and alumina is also considered as an alternative. Alumina toughened zirconia (80 wt% ZrO2, 20 wt% Al2O3) showed improved ageing resistance in comparison to 3Y-TZP itself [87]. In the presence of a temperature change, the tendency of zirconia for a phase-change makes it quite challenging to process it with a method like PBSLP which includes rapid heating and cooling cycles. Various studies were carried out in order to manufacture zirconia materials by PBSLP with obtaining desired phases and compositions at the end.

Direct PBSLP of zirconia is always an attractive approach for scientist and manufacturers as it requires less process steps and energy. That means obtaining solid, dense pieces in a single lasering step without any following de-binding process could be very cost-effective and rapid method for manufacturing. Unfortunately, the number of cases that come closer to success is very low due to various challenges in working with ceramics in general. First case on PBSLP of plain YSZ powder was reported by Bertrand et al., in 2007 [88]. In that study, five different compositions of YSZ were studied and the most satisfying results obtained with Zircar ZYP30 (10 wt%) atomized powder. The final density of the pieces was 56% and a post treatment trial in a conventional furnace (max. temperature 1200 °C) did not improve the density of pieces. In the same year, Shishkovsky et al. studied the effect of different laser irradiation conditions on direct PBSLP of YSZ/alumina (YSZ; ZrO$_2$ 90 wt%, Y$_2$O$_3$ 10 wt%, from Zircar Zirconia Inc., and the alumina Al$_2$O$_3$ from Baikowsky Inc. In the ratio of 4:1) and YSZ/aluminum (ADC4 grade)
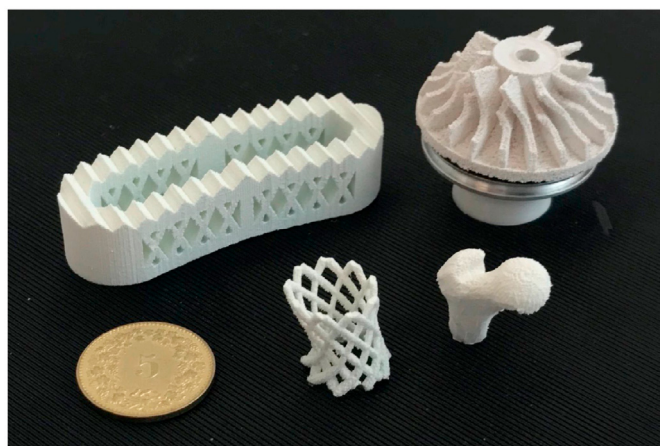


**Fig. 8.** Alumina toughened zirconia based pieces produced by Verga et al. with combination of PBSLP and thermally post-treatment [95].

mixture in oxygen and argon environment [89]. They proved that after direct PBSLP of YSZ/aluminum blend, alumina ($Al_2O_3$) was formed even in the argon environment. That refers to decomposition of zirconia under these printing conditions and possible creation of the intermetallic Al3Zr phase. However further phase study was required. Similar to the previous study, a structure that is relatively dense but with cracks and low mechanical properties was obtained. In order to improve mechanical properties, J. Wilkes et al. developed a high temperature pre-heating system [90]. In this way, they were able to minimize the thermal gradient and prevent the occurrence of thermally induced stresses. A mixture of 41.5 wt% Y-TZP (6 wt% yttria stabilized) and 58.5 wt% alumina (the eutectic blend ratio of alumina-zirconia-yttria system) was used [91]. The preheating temperature was selected at 1715 °C, which is slightly below the eutectic melting temperature (1860 °C). In addition to the study of Hagedorn et al. [92], the comparison of preheated and non-preheated samples was done in terms of density, mechanical property and surface finishing. With preheating, it was possible to print ceramic pieces with almost 100% density without any additional sintering and post-processing. The crack-free final structure consists of fine-grained two-phase combination of tetragonal zirconia and alpha-alumina. While the flexural strength of pieces was above 500 MPa, the surface quality was pretty low due to the low viscous melt pool that exceeds the boundaries of the scanned part and wets the surrounding powder. The effect of pre-heating was also investigated by Liu et al. [93] With the intention of reducing crack propagation and increasing the powder flowability, a coarse blend of two size diameters; 22.5–45 μm (80 wt%) and 9–22.5 μm (20 wt%) of yttria stabilized zirconia ($ZrO_2$ –7 wt.% $Y_2O_3$) was used. With help of secondary lasers introduced into the system, pre-heating applications at 1500, 2000 and 2500 °C were tested. It was possible to reduce the thermal gap between two continuous laser applications which results in crack reduction in the structure. It was also possible to maintain desired phases, for example the tetragonal phase, by keeping the powder bed in a certain temperature range and preventing the phase transformation. However, pre-heating system could not be used effectively due to some hardware limitations. In 2018, Ferrage et al. has got back to the direct PBSLP of plain YSZ powder and used 8Y-TZP due to its cubic stabilized structure that is more stable for thermal applications [94]. The laser absorbency of 8Y-TZP powder was increased from 2% to almost 60% by physical mixing of 0.75 wt % graphite. With increased absorbency and optimized processing parameters, an efficient laser-matter interaction was obtained that results in manufacturing 8Y-TZP pieces with relative density of 96.5%. However, the microstructure of manufactured pieces showed a columnar structure in the direction of printing which is not observed in conventionally produced pieces. They were also rich in cracks and showing a low mechanical strength. Lately, Koopmann et al. has investigated the PBSLP processing of ceramic-metallic multi-materials as a combination of 1.2367 (X38CrMoV5-3) tool steel and alumina toughened zirconia ($ZrO_2$ 80%) [95]. Optimum lasing parameters were determined for 10 mm³ ceramic pieces as the laser power of 90 W, scanning velocity of 200 mm/s, hatch distance of 160 μm, and layer thickness of 50 μm. Final relative density of pieces was determined as 94%. Processed pieces showed four different microstructures under SEM imaging due to different cooling rates and unmolten zirconia powder particles. Recently in 2020, Verga et al. has proven a novel method to enhance the laser-matter interaction in direct PBSLP [96]. An aqueous dispersion of 80 wt% of yttria-stabilized zirconia and 20% α-Alumina was prepared with addition of 4 wt% of dispersing agent (Dolapix CE64 – Zschimmer & Schwarz, DE) and 0.1 wt% of binder (Optapix KG1000–Zschimmer & Schwarz, DE). After a number of milling processing, granulates were produced by spray drying method with fine fraction ($D_{10}$ = 5 μm; $D_{50}$ = 11 μm; $D_{90}$ = 34 μm). As an innovative approach, the powder granulates were calcined under a reducing atmosphere (98% Ar-2% $H_2$) at 650 °C and a homogenous distribution of carbon in the structure was obtained. The laser-matter interaction was increased as a result of darkened color. Pieces were produced with a continuous wave (CW) 200W Nd-YAG fiber laser. Best results were obtained with 34 W laser power, 86 mm/s scanning velocity, hatch distance of 0.175 mm and layer thickness of 0.04 mm. The contribution of a possible post thermal treatment to direct PBSLP was studied with help of a dilatometer. Pieces showed better mechanical performance due to reduced cracks in the structure after a treatment in 1300 °C from 2 to 10 h. This study has demonstrated the possibility of producing ceramic parts by direct PBSLP with help of additional post thermal treatments.

In order to prevent crack formation and improve mechanical properties, indirect PBSLP methods are developed and applied. In these methods, the green body of pieces were obtained by sintering the sacrificial binder (mostly polymers) addition in low temperatures. Then, this sacrificial binder (can remain in the structure in few cases) is eliminated by post-processes such as debinding, and the final density of the pieces is obtained. Introducing the binder into the structure was commonly done with two methods. Shahzad et al. formed a powder composition consisting of polypropylene (PP) and 3Y-TZP (Tosoh) by thermally induced phase separation [97]. In the first attempt, the density of indirect PBSLP processed parts was only 32%, however, it was improved up to 54% by pressure infiltration (PI) at 16 MPa with a 30 vol% $ZrO_2$ suspension. As a final step, pieces were processed with warm isostatic pressing (WIP) in addition to PI, and final density of 85% was obtained for ceramic pieces. However, cracks were observed in the final structure. Additionally, the best mechanical strength was obtained with 70 vol% polymer concentration. In another study, a composite powder blend of 3Y-TZP/MgO and epoxy resin E12 was obtained by mechanical mixing of three powders [98]. Indirect PBSLP process was carried out by following parameters of laser power = 7 W, scanning speed = 2600 mm/s, hatch spacing = 0.15 mm and layer thickness = 0.09 mm. Thanks to the indirect processing, green bodies were obtained with less energy density than direct PBSLP. Indirect PBSLP processed samples were densified by cold isostatic pressing (CIP) and sintered at 1500 °C. Finally, 3Y-TZP ceramic pieces were obtained with relative density of 86.65% (Fig. X). Similarly, Shi et al. combined PBSLP with CIP in order to obtain dense zirconia parts. In their study, nano-zirconia powder is coated by the nylon 12 binder by solvent precipitation method [99]. SLP processing was followed by subsequent CIP at 200 MPa. At the end, relative density of 97% and Vickers Hardness of 1180 HV were obtained after a proper furnace sintering. To conclude this section, it can be said that manufacturing solid and dense zirconia parts without any pre and past processes is still an area to be developed. Even the nature of zirconia in terms of thermal behaviors and laser-mater interaction is a limitation, additional processes like pre-heating or binder based 2 step sintering can help to improve the properties of final pieces (see Fig. 8). On the other side, further studies on stabilizing of zirconia might reveal new zirconia-based compositions to be used in a laser including process like PBSLP (Table 4).

### 4.4. Alumina

The name alumina is used to describe the pure $Al_2O_3$ ceramic, although many commercially available aluminas have less than 98%, and the term corundum refers to the mineral, both for the alpha phase [100]. Doping the alumina structure may lead to color/properties changes and other names may be adopted (ex.: Sapphire - Ti+4/Fe+2 ions - and Ruby - Cr+3 ions).

Alumina is a widely used ceramic on the planet, produced mainly in China, Australia, Brazil and India [101]) and it is considered a structural ceramic. Structural ceramics often have or several good properties, such as: high hardness, chemical inertness, high temperature mechanical strength, wear resistance, among others interesting properties for industry.

Alumina, specifically, is widely used in several areas of industry. Its main properties when compared to other structural ceramics are high hardness, wear resistance (ex.: seal faces for rotary water pumps), low thermal conductivity (ex:. refractories) and high temperatures work range (1850 - 1950 °C for crucible and furnace materials) [100]. Some applications may use Alumina for its inertness and low reactivity.

13

**Table 4**
Summary of the process conditions and final properties of sintered zirconia-based parts by PBSLP.

| Ref. | Year | Powder feedstock | Laser & strategy | Post-processing | Properties of processed parts* |
|------|------|------------------|------------------|-----------------|-------------------------------|
| Bertrand et al. [88] | 2007 | Zircar ZYP30 (10 wt %)<br>Particle Size:<br>$<10^{-6}$m | Phenix Systems PM100 (50W)<br>V = 1250–2000 mm/s<br>defocalisation: 6 to 12 mm<br>hatch distance: 20–40 μm | No Post Processing | 1 cm$^3$ zirconia cubes with 56% density |
| Shishkovsky et al. [89] | 2007 | Y-TZP; ZrO$_2$ 90 wt%, Y$_2$O$_3$ 10 wt%, Zircar Zirconia Inc and, ADC4 grade aluminum and Al$_2$O$_3$ from Baikowsky Inc. In the total ratio of 4:1 | Phenix Systems PM100 (50W)<br>defocalisation: ~6 mm<br>Laser spot size, D: ~80 μm hatch distance: 20–40 μm,<br>in air. | No Post Processing | No specific information |
| Wilkes et al. [90] | 2013 | Al$_2$O$_3$–ZrO$_2$ blends<br>41.5 wt% ZrO$_2$, 58.5 wt% Al$_2$O$_3$<br>80 wt% ZrO$_2$, 20 wt% Al$_2$O$_3$<br>Y-TZP; ZrO$_2$ 94 wt%, Y$_2$O$_3$ 6 wt% in processes including pre-heating p. size approx. 20–70 μm | Nd:YAG-laser (150 W) for processing<br>CO$_2$-laser (1000 W) for pre-heating | No Post Processing | Pieces with almost 100% density with help of pre-heating around (1600 °C). Various outcomes with different ratios of Al$_2$O$_3$–ZrO$_2$ blends<br>Flexural strength around 500 MPa. |
| Hagedorn et al. [92] | 2010 | 41.5 wt% Y-TZP (ZrO$_2$ 94 wt%, Y$_2$O$_3$ 6 wt%), 58.5 wt% Al$_2$O$_3$ | Layer thickness of 50 μm,<br>Scanning velocity of 200 mm/s,<br>Laser power of 60 W,<br>Scanning offset of 50 μm,<br>Time gap of 60 ms between two subsequent scanning vectors<br>Pre-heating around 1860°c | No Post Processing | 2.5 mm x ø18 mm specimens with density of 100% without any cracks. |
| Liu et al. [93] | 2015 | Yttria Stabilized Zirconia (ZrO$_2$ –7 wt.% Y$_2$O$_3$) a blend of; 22.5–45 mm (80 wt%) and 9–22.5 mm (20 wt%) | MCP Realizer SLM 250, Germany | Post Thermal Treatment at 1500, 2000, and 2500 °C | The relative density of 91% can be reached with increasing pre-heating (1–2% difference between set-ups) |
| Ferrage et al. [94] | 2018 | 8YSZ (ZrO$_2$–8Y$_2$O$_3$) d$_{10}$ of 3 μm, d$_{50}$ of 14 μm, and d$_{90}$ of 50 μm<br>+ <2 wt% graphite powder (various trials) | Phenix ProX 200 Nd:YAG<br>Laser power (W): 78-87<br>Lasing speed (V): 60–75 mm/s<br>Hatch distance (d): 50 μm<br>Layer thickness (th): 100 μm<br>Compaction rate (C): 300% | No Post Processing | Reproducible pieces with relative density around 96.5%, however with low mechanical strength |
| Koopmann et al. [95] | 2019 | ATZ (80 wt % ZrO$_2$, 20 wt% Al$_2$O$_3$) | Realizer SLM 125 equipped with Nd:YAG laser<br>Laser power (W): 90<br>Lasing speed (V): 200 mm/s<br>Hatch distance (d): 160 μm<br>Layer thickness (th): 50 μm | No Post Processing | 10 mm × 10 mm X 10 mm pieces showed relative density above 94% with tensile strength around 20.4 ± 4.6 MPa. |
| Verga et al. [96] | 2020 | ATZ granulates of 80 wt% of yttria-stabilized zirconia (D$_{10}$ = 1 μm; D$_{50}$ = 2.5 μm; D$_{90}$ = 5 μm)<br>+20 wt% of α-Alumina (D$_{10}$ = 0.09 μm; D$_{50}$ = 0.17 μm; D$_{90}$ = 0.43 μm) calcination under a reducing atmosphere (98% Ar-2% H$_2$) at 650 °C for 2 h | CW 200W Nd-YAG laser (redPOWER, SPI Lasers Ltd, UK)<br>Laser power (W): 34<br>Lasing speed (V): 86 mm/s<br>Hatch distance (d): 0.175 mm<br>Layer thickness (th): 0.04 mm | Post Thermal Treatment at 1300 °C for 2–10 h. | Especially with thermal treatment the density and mechanical strength of pieces were increased. Shrinkage of pieces was observed with increasing treatment time |
| Shahzad et al. [97] | 2014 | 3Y-TZP (3 mol% Y$_2$O$_3$) and isotactic polypropylene (PP) | CO2 laser (λ: 10.6 μm) with power of 100W and spot size 400 mm. | Warm Isostatic Pressing at 64 MPa and at 135 °C for 5 min<br>Debinding heating rate 0.1 °C/min in air to 600 °C<br>Sintering in air at 1450 °C for 2 h | |
| Chen et al. [98] | 2018 | 3Y-TZP (3 mol% Y$_2$O$_3$)<br>+0.5 wt% MgO powder (sintering aid)<br>+6.0 wt% epoxy resin E12 (sacrificial resin) | CO2 laser (λ: 10.6 μm) with power of 100W<br>Laser power (W): 7<br>Lasing speed (V): 2400–2800 mm/s<br>Hatch distance (d): 0.15 mm<br>Layer thickness (th): 0.09 mm | Cold Isostatic Pressing at 280 MPa for 5 min at room temperature through liquid medium (kerosene) | With the optimum sintering temperature at 1500 °C pieces had the highest flexural strength of 279.50 ± 10.50 MPa and the maximum densification of 86.65 ± 0.20% |
| Shi et al. [99] | 2014 | ZrO$_2$ + nylon 12 | Energy density: 0.415 J/mm$^2$<br>Laser power: 6.6 W<br>Hatch distance (h): 0.1 mm | Cold Isostatic Pressing at 200 MPa<br>No information for conventional sintering | Relative density of final pieces around 97% and Vickers Hardness of 1180 HV |

**Table 5**
Summary of the process conditions and final properties of sintered Alumina parts by PBSLP.

| Ref. | Year | Powder feedstock | Laser & strategy | Post-processing | Properties of processed parts* |
|------|------|------------------|------------------|-----------------|-------------------------------|
| [103] | 1995 | Alumina (65–75%) + Aluminum | Nd:YAG 40 W 20 kHz:<br>Scan speed 8.5–40 mm/s<br>Line spacing 250 μm<br>$CO_2$ 16 W 5 kHz<br>Scan speed 15–40 mm/s<br>Line spacing 125 μm | 45% R.D. | Heat treatment to oxidize residual Aluminum and strengthening |
| [104] | 1995 | Alumina + PMMA + $SiO_2$ + n-but-MA | $CO_2$ 6–14 W<br>Scan speed 300–1500 mm/s<br>Line spacing 75–125 μm | 60% R.D. | Infiltration w/alumina sol + T.T. |
| [105] | 1997 | Alumina (40–90%) + glasses + $B_2O_3$ | $CO_2$ 15 W (N2 atm)<br>Scan speed 560 mm/s<br>Line spacing 125 μm layer thick. 200–250 μm | 1.7 g/cm$^3$ max | T.T. |
| [114] | 1998 | Developing $HBO_2$ as binder for Alumina | – | – | T.T. |
| [115] | 1999 | Alumina + $B_2O_3$ + (SiO2 and $Cr_2O_3$ infiltrators) | $CO_2$ 14–16.5 W<br>Scan speed 320–1190 mm/s<br>Line spacing 125 μm layer thick. 200–250 μm | 80% R.D. | infiltration + T.T. |
| [116] | 2001 | Alumina + $B_2O_3$ + ($Al_2O_3$ infiltrators) | $CO_2$ 14–16.5 W<br>Scan speed 320–1190 mm/s<br>Line spacing 125 μm layer thick. 200–250 μm | 2.25 g/cm$^3$ max | infiltration + T.T. |
| [117] | 2002 | Alumina + $B_2O_3$ | $CO_2$ 14–16.5 W<br>Scan speed 320–1190 mm/s<br>Line spacing 125 μm layer thick. 200–250 μm | 1.1 g/cm$^3$ max | T.T. |
| [89] | 2007 | Alumina (~80%) + Stearic acid | $CO_2$ 4–6.2 W<br>Scan speed 889 mm/s<br>Line spacing 127 μm | 88% R.D. | T.T. |
| [106] | 2010 | Alumina (58.5%) + 6YSZ | $CO_2$ pre-heating<br>Nd:YAG<br>Scan speed 200 mm/s<br>Line spacing 50 μm layer thick. 50 μm<br>spot size 200 μm | 56% R.D. | – |
| [118] | 2011 | Alumina (58.5%) + 6YSZ | $CO_2$ pre-heating 1600+<br>Nd:YAG 48–60 W<br>Scan speed 200 mm/s layer thick. 50 μm<br>spot size 200 μm | 56% R.D. | – |
| [108] | 2012 | Alumina (40%) + Polyamide | $CO_2$ 5 W<br>Scan speed 600 mm/s<br>Line spacing 150 μm layer thick. 150 μm | 48–68% R.D. | T.T + different pressing + infiltration |
| [107] | 2012 | Alumina + Epoxy | $CO_2$ 10–14 W<br>Scan speed 1600–2000 mm/s<br>Line spacing 70–130 μm layer thick. 80–120 μm | 57% R.D. | CIP |
| [110] | 2012 | Alumina (22%) + Polyamide | $CO_2$ 3–7 W<br>Scan speed 400–1250 mm/s<br>Line spacing 150–350 μm layer thick. 100 μm | 94,1% R.D. | CIP + T.T. |
| [119] | 2012 | Alumina (40–50%) + Polyamide | $CO_2$ 3–7 W (N2 atm)<br>Scan speed 100–1257 mm/s<br>Line spacing 150–300 μm layer thick. 150 μm | 50% R.D. | T.T. |
| [120] | 2012 | Alumina (40–50%) + Polyamide | $CO_2$ 3–10 W<br>Scan speed 600–1250 mm/s<br>Line spacing 150–350 μm layer thick. 150 μm | 64% R.D. | CIP/QIP + T.T. + infiltration |
| [24] | 2013 | Alumina 91% + PP | $CO_2$ 5 W<br>Scan speed 875 mm/s<br>Line spacing 150 μm layer thick. 200 μm | 89% R.D. | WIP + Infiltration + T.T. |
| [109] | 2013 | Alumina (61%) + PS | $CO_2$ 13–17 W<br>Scan speed 600–1200 mm/s<br>Line spacing 100–200 μm layer thick. 250 μm | 66% R.D. | WIP + Infiltration + T.T. |

**Table 5** (*continued*)

| Ref. | Year | Powder feedstock | Laser & strategy | Post-processing | Properties of processed parts* |
|---|---|---|---|---|---|
| [111] | 2013 | Alumina coated PVA | $CO_2$ 15–20 W<br>Scan speed 1600–2000 mm/s<br>Line spacing 100–140 µm layer thick. 150 µm | 94,5% R.D. | CIP/HIP + T.T. |
| [121] | 2013 | Alumina (30–39%) coated PS | $CO_2$ 10 W<br>Scan speed 500–1000 mm/s<br>Line spacing 100–300 µm layer thick. 250 µm | – | – |
| [112] | 2014 | Alumina (99.7%) + $Na_2O$ + $Fe_2O_3$ + $SiO_2$ + $B_2O_3$ | $CO_2$ 30 W<br>Scan speed 2000 mm/s<br>Line spacing 200 µm layer thick. 150 µm | – | T.T. |
| [122] | 2018 | Alumina (91–99%) + $B_4C$ | $CO_2$ 5–60 W<br>Scan speed 20–6000 mm/s layer thick. 100 µm | 27% R.D. | T.T. |
| [123] | 2018 | Alumina (99,8%) + $Na_2O$ + $Fe_2O_3$ + $SiO_2$ + MgO +<br>$TiO_2$ + CaO<br>Slurry system with $H_2O$ | IPG YLR-500 fiber laser 100–200W pre-heating<br>Scan speed 60–120 mm/s<br>Line spacing 50 µm layer thick. 50 µm | – | – |
| [124] | 2018 | Alumina coated PS<br>Single layer tests | Nd:YAG 2–7 W<br>Scan speed 5–50 mm/s<br>Line spacing 50 µm layer thick. 2000 µm | 81.3% R.D. | Suggests T.T. for further tests |
| [125] | 2018 | Alumina<br>Alumina substrates<br>Single track study | Fiber laser 100–400 W<br>Scan speed 300–1000 mm/s<br>Line spacing 50 µm layer thick. 250 µm | – | – |
| [102] | 2018 | Alumina (99,8%) + $Na_2O$ + $Fe_2O_3$ + $SiO_2$ + MgO +<br>$TiO_2$ + CaO<br>Slurry system with $H_2O$<br>Crack study in one layer | IPG YLR-500 fiber laser 55-20W pre-heating<br>Scan speed 90 mm/s<br>Line spacing 50 µm layer thick. 50 µm | – | Same as [123] |
| [126] | 2019 | Alumina + Epoxy | HK-C250 8 W<br>Scan speed 1500 mm/s<br>Line spacing 100 µm layer thick. 150 µm | – | T.T. |
| [113] | 2020 | Alumina (90%) + Epoxy<br>Porosity as objective | Laser 6–8W<br>Scan speed 1600–2000 mm/s<br>Line spacing 110–150 µm | – | – |

The medical industry makes use of alumina (nearly inert bioceramic) to build prosthetics implants, considering that it is chemically and biologically suitable for such purposes and has satisfactory characteristics for a long duration use. Alumina was first suggested as biomaterial for applications in medicine in 1932 and the first hip implant using alumina was done in the 1970s [100]. More than a million alumina components were used in hip prostheses to date.

Alumina also fits in many electric/electronics applications, considered vital for any high temperature and electrical insulation. Vastly used in the microchip and electronics components industry, its high electrical resistivity and low dielectric constant are of most value in these applications [100]. The electrical resistivity (as also the sintering temperature) may be adapted by adding a second phase (ex.: silicates) to the composition [100].

There is also much technological interest in alumina by the military (body armors enhancement, bullet proof systems), jewelry (rubies and sapphires) and general components (pipes, machining, cutting, etc) [100].

In order to obtain dense parts using alumina, it's necessary to use a combination of optimized factors (particle size, high density green part, post-processing steps, etc). In addition, Alumina has a high range of sintering temperatures. Mainly for this last reason, selective laser sintering/melting of pure alumina is a technological challenge. The temperatures can be reached, but the higher is the temperature range, the higher is the associated residual stresses. Crack formation and other defects are also favored by a greater change in temperature in a short space of time [102].

The first solutions to make parts using SLS/M for alumina were to add a vitreous phase component, in order to facilitate the manufacturing and consolidation of each layer with less critical consequences. Metallic aluminum [103], PMMA [104], B2O3 [105], Stearic acid [89], zirconia [106], epoxies (Fig.) [107], polyamides [108], polystyrenes [109] and other oxides were used to allow the production of pieces using alumina (Table 5). However, these strategies often required several post-processing steps and the final piece hasn't the final mechanical properties as high as it is needed for some high technological purposes. Relatively-high density was obtained (>94%), using post-processing methods, for strategies using polyamides [110] and PVA coating [111].

A possibility to avoid the addition of a vitreous phase is to use an absorbance enhancer, in the case of a fiber laser, in order to allow the alumina powder to properly absorb the energy emitted by the laser and sinter/melt each layer [112].

Another strategy is to use a reactive approach. Instead of using the final phase/form of alumina for powder bed forming, a precursor is used. For example, aluminum hydroxide. During the laser exposure the hydroxide, inside an atmospheric chamber, transforms into alumina and diffusing the energy absorbed differently. It may allow a better consolidation of the final solid piece.

PBSLP of pure alumina is still a challenge. Considering the commercially used range of 98% of purity, there is place to work on the printability optimization through the 2% left in the composition. These 2% may contemplate any component, organic or inorganic, but it may allow the manufacturing of a piece with final properties near to the conventional methods. The challenge is to find a compromise between the characteristics needed to have a printable alumina powder and the final properties obtained (see Fig. 9).

## 5. Discussions

### 5.1. Limitation of printability of material and existing answers

Considering all steps to build a piece by PBSLP, from ceramic powders feedstock to a final piece, several limitations can be observed. The global behaviour of PBSLP is unique for each combination of a given ceramic powder and a PBSLP machine. For example, manufacturing an Alumina piece using a machine A and manufacturing Zirconia with a machine B



**Fig. 9.** Green bodies of Al2O3 PHM Ceramics, before debinding process [113]. (For interpretation of the references to color in this figure legend, the reader is referred to the Web version of this article.)

have their own specific challenges, although some common issues may often be presented.

In order to improve the chances of building highly dense parts, a well-packed powder bed seems to be necessary. Two important factors that contribute to form and spread the powder bed are the flowability and the packing density [127–129]. Usually, to control those factors, powders with high flowability and optimized granulometry combinations are sought. The most often used strategy to try to obtain a good compromise of both is to use spherical and dense particles [130], which is also used to simulate the laser interactions with ceramic particles [131]. The use of irregular shaped particles may create non-uniform regions on the powder bed and also lower the flowability and packing density [132]. It is also possible to estimate the final packing density of a mixture of different particle size powders, in order to have an optimal theoretical packing [133]. Improving the packing density, by using bimodal powder mixtures, may also improve the flowability, the sintered density and, in some cases, reduce shrinkage [134].

Ceramic powders with different compositions are going to interact, i.e. absorb/reflect, differently according, not only to the wavelength of the laser in question (Table 6), but the selected power, spot size, angle, focalization, lasing speed and strategy [135]. Yet, although one can possibly adapt the powder (with additives or dopants, for example [136]) to interact better with a given laser, it might be a challenge in certain cases where high purity is expected. The additive manufacturing community are still working with a small variation of lasers, among the most used $CO_2$ and Nd:Yag lasers [125].

When the powder processing starts, with the first interactions between the laser and the powder particles, the building platform must be chosen accordingly. It means that the used ceramic powder, under the selected lasing conditions, must have the best interaction/adhesion possible to the building platform. The fixation of the first layers is essential to a proper manufacturing. The amount of pieces produced in

**Table 6**
Absorbance (A) of ceramic powders under Nd-YAG ($\lambda = 1.06\ \mu m$) and $CO_2$ ($\lambda = 10.6\ \mu m$) lasers [137,138] (*measured by authors of this review).

| Material | Nd-YAG ($\lambda = 1.06\ \mu m$) | $CO_2$ ($\lambda = 10.6\ \mu m$) |
|---|---|---|
| ZnO | 0.02 | 0.94 |
| Al2O3 | 0.03 | 0.96 |
| SiO2 | 0.04 | 0.96 |
| BaO | 0.04 | 0.92 |
| 8YSZ | 0.02 | – |
| CuO | 0.11 | 0.76 |
| HA | 0.03* | – |
| TiC | 0.82 | 0.46 |
| SiC | 0.78 | 0.66 |

the same platform have an influence on the heat homogeneity through the platform and the samples [139]. Platforms with different materials can be used, as also prepared with ceramic coatings, surface patterns, roughness levels, etc [125]. The understanding of the phenomena between the chosen surface/building platform and the ceramic powder is of prime importance. The greater limitations are the commercial availability or the access to test different alternatives of building platforms.

The strategy of using compatible (or the same) material as the ceramic powder to be manufactured, over the platform as coating or a thin base film, may overcome some adhesion/diffusion phenomena [125].

Sometimes researchers have limited access to the machine parameters, regarding mainly to the lasing settings and building time frames. Controlling the laser optical specifications allow the user to take specific actions towards the laser beam interaction with the matter. The possibility to control all the laser parameters allows a proper testing and adaptation in specific situation, for example, to suspend the building process to change/adapt the laser parameters and then continue with another set. This might open working window to adapt to heat flows that vary with the height of the piece, or to build multi-layer materials. Sometimes it would be necessary to change the lasing parameters during processing, however not all commercial SLP machines offer that condition to the operator. The studies conducted using machines that allow the operator to control more parameters have the capacity to explore the phenomena more broadly [138].

### 5.2. Real-time in-line measurements

In such a manufacturing method like selective laser processing, the measurement of the real time temperature is critical. During a sintering/melting process, it is a great advantage to be able to track the reached temperature around interacting particles, in order to control the formation/transformation mechanisms of existing phases [19]. While ceramic materials are being processed under the laser, the temperature of the interaction zone increases and then decreases rapidly. That might result in phase changes or forming of new ones, affect the speed of phase transitions, chemical reactions, microstructure, and properties of the material. However, it is a clear fact that will be significantly different compared to conventional methods, due to the changes in heating/cooling rates. Temperature distribution and monitoring at the laser-matter interaction zone is mostly carried out by two different methods, physical measurements with thermal detectors such as thermocouples or semiconductor bolometers, and optical imaging with IR cameras and also with pyrometers [106]. Use of thermocouples are not preferred commonly any more due to their low sensitivity to rapid heat changes and slow response time. Also, many of the selective laser processing equipment in the market today are designed and manufactured for polymer and metal use and they are not eligible to be modified to insert thermocouples. Another challenge with working with thermocouples is the reached temperature during ceramic processing. While extreme temperatures (above 2000 °C) can be reached during ceramic powder processing, a thermocouple correctly processing at that temperature is most likely impossible [140].

On the other side, a contactless method such as pyrometric measurement can process at that point. However, the use of pyrometer in a laser-based manufacturing brings a number of methodological problems with it. Most significantly, the correct measurement of the thermal radiation is required in order to avoid the superposition of the thermal radiation by considering different types of noise. Additionally, consideration of laser action-based elements such as reflected laser beam, radiation of the laser-induced plume, and thermal radiation from the heat-affected zone is critically important [141]. Modern infra-red cameras are another contactless method to monitor thermal distributions on the laser-mater interaction spot with a higher spatial and temporal resolution in comparison to pyrometers. However, it is extremely challenging to calculate the brightness temperature values because the emissivity changes in a wide spectral window

during such a process like SLP. Even if the brightness temperature was calculated before with a monochromatic pyrometer, the value of emissivity should be known for a proper measurement. Need for higher energy densities, high reflectivity and low absorbency of ceramic materials make it even harder to calculate the true temperature. A system including both 2D monochromatic pyrometer and a multi-wavelength pyrometer, and an infra-red camera has been used by Smurov et al. [141] However, this process was done for SLP of metallic material, thus, a number of modifications are needed to be done in ceramic processing.

### 5.3. Standards needs

Standardization of the additive manufacturing would provide a wider adoption of this technology and best practices, regulations and benchmarks for industries and research organizations. However, for this emerging and disruptive technology like 3D printing, standardization is not straightforward. Specifically, in terms of selective laser melting/sintering there are three main standards that refer to the terminology used in these techniques, ISO/ASTM 52900 "Additive manufacturing — General principles — Terminology", ISO/ASTM 52911–1:2019 "Additive manufacturing — Design — Part 1: Laser-based powder bed fusion of metals" and ISO/ASTM 52911–2:2019 "Additive manufacturing — Design — Part 2: Laser-based powder bed fusion of polymers". However, these standards, in addition to the fact that there is no specific one for ceramics, do not specify a single term to be used for each technique, suggesting several options for the same technique, as indicated in the document, powder bed fusion, also called SLS, SLSM …

Apart from the lack of a single standard for the terminology of this technique, nor is it specified standards for bulk raw ceramics requirements (powder particle size and distribution, flowability/pourability, morphology, density, flowability ceramic grains). The creation of standards for ceramics would allow the repeatable production of ceramic parts with high quality. Moreover, this technique depends on many complex variables, starting from raw materials to design the manufacturing process by optimizing the interaction between the software and hardware.

Standardization can help to define the parameters for each step of AM production, helping to create a consistent process every step of the way. This ensures that the desired quality outcome is achieved. Moreover, this technique is used in highly regulated industries such as aerospace, defense and medical where parts have quite different properties and the qualification and certification will provide a guideline against which parts are assessed and qualified.

### 5.4. Future and challenges of AM and PBSLP of ceramics

Companies are investing efforts to be the leaders of their respective fields in this race of AM market. Patent applications for AM increased at an average rate of 36% from 2015 to 2018 (according to European Patent Office (EPO)), more than ten times the average annual growth of all applications at the EPO during the same time (3.5%). Been U.S. companies the ones with the higher number of patent applications (35%). Even if ceramic AM has recently experimented an increase in its development, it is still in an early stage compared with metal or polymer AM. It is due to the high materials costs and deficiencies in ceramic parts by the existing challenges during the printing process that its adoption is been delayed in the market, showing a market size lower than 200 million euros in 2019 [142].

However, research and development activity to improve the mechanical and performance properties of shaped ceramic parts is increasing rapidly and continued adoption is driving the cost of materials down. According to recent forecasts and because of the current speed of technological advancements, it is expected that the AM ceramics industry will reach maturity in 2025, achieving a market size of EUR 3.3 billion (USD 3.6 billion), with opportunities in the aerospace, automotive, electronics, energy, marine, and medical segments.

In this review, we explained that every step on the PBSLP print affects the final properties of the shaped parts at the end of the process. Then, the improvement and future of the technique can come from the adjustment of any of the variables presented on the technique such as powder properties and composition, machine technical design, process parameters, and post-treatments. As PBSLP is already well implemented for polymeric and metallic materials it is logic to think that future innovations will be first developed thinking in these materials and from there be adapted for ceramics. Recently, Roy et al. [143,144] patented a new micro-AM process called micro-scale selective laser sintering (μ-SLS) able to produce metal parts with a feature resolution with sub-5μm and a throughput of greater than 60 mm³/h. A redesign of the conventional PBSLP apparatus and the use of nanoparticles were needed to be able to produce the submicron particle bed and print at high throughput. This innovative technology could eventually allow the fabrication of complete microelectronic parts and subsequently, be also used for the production of microscale ceramic parts.

The company Sintratec developed different patents on the modification of the PBSLP devices that can perfectly serve as examples of innovations improving the process performance. A heating device located under the building platform that makes it possible to control the heat distribution of the powder bed during the printing process accelerating and improving the printing process [145]. Another patent refers to a PBSLP device with a movable beam generation unit allowing to always keep the same angle of the laser respect to the powder bed surface during the printing process [146]. Another patent shows a PBSLP device with a replaceable raw material processing unit, making realizable the change of the raw material in a faster way, speeding up the process [147].

These are some examples of how fast the development of AM technology is, as PBSLP during the last years. This technology has a great potential for future progress and the number of industries profiting of it is increasing. Industries as automotive, medical, and aerospace are leading the use of this technology and will be responsible for its expansion into the future.

## 6. Conclusion

Powder bed selective laser processing is a promising method for the manufacturing of ceramics including calcium phosphate, silicon carbide, zirconia, alumina, and their composites for various industrial applications. In comparison to other additive manufacturing methods, PBSLP can present preferable features such as higher manufacturing speeds and need for less post-processing. In today's market, various PBSLP machines can be found that are already operating for metals and polymers mostly. Adapting this equipment to use for ceramic manufacturing requires considerable modifications and research.

A good understanding of laser-matter interaction is critically important in order to obtain better control of the printing process in terms of tuning the energy density transferred to the powder bed, the control of porosity, and the improvement of mechanical properties by reducing the thermal stresses.

The improvement of PBSLP of ceramics relies, partially, on the comprehension of the powder bed formation and packing during the process. Computational simulations may present a solution to foresee an ideal morphology for a given powder, which allows to adapt factors like flowability, format and density of the ceramic particles for PBSLP. Tailoring the ceramic particles to optimize the powder bed will directly affect the laser parameters, considering that the format, size, organization (packing) and nature of the ceramic particles will create a unique laser/ceramic interaction. In addition to this laser/ceramic interaction, there is a building platform/ceramic interaction that takes place during the consolidation of the first layers. The adhesion of the piece to the building platform and the heat-flow through the platform during PBSLP are two examples of impactful factors of the building platform/ceramic interaction. Such interactions may be also studied previously using computational methods, since one has the necessary knowledge of the ceramic powder's and the involved materials properties.

Measuring the heat variation during PBSLP is still a challenge. Measurements using physically inserted devices like thermocouples are mostly incompatible with the environment inside the building chamber. However, contactless systems, like pyrometers, may be a compatible solution to measure the real-time and fast temperature changes during the laser/matter interactions. Some modifications and optimizations continue to be necessary in order to build a pyrometer system adapted to ceramic processing, i.e. greater energy densities, high levels of reflectivity and, eventually, the low absorbance of the laser energy.

Standardization of the whole PBSLP method for ceramic materials is a safe mechanism to additive manufacturing community in general. The specifications that a standard can assure about the methodology are a consistent strategy to ensure a base line of higher quality products and research. Towards having new software and hardware, the standardization of the process might give direction to new machinery development.

Interest and investments in the additive manufacturing industry and research are growing consistently in the past few years. Still, additive manufacturing products still needs development in all stages: raw material, processing, post-processing, standards, simulation and machinery. Naturally, the development of all these stages is more advanced for polymeric materials first, metallic materials secondly and, for all the intrinsic challenges, ceramic materials for last.

## Declaration of competing interest

The authors declare that they have no known competing financial interests or personal relationships that could have appeared to influence the work reported in this paper.

## Acknowledgements

## References

[1] Z. Chen, Z. Li, J. Li, C. Liu, C. Lao, Y. Fu, C. Liu, Y. Li, P. Wang, Y. He, 3D printing of ceramics: a review,, J. Eur. Ceram. Soc. 39 (2019) 661–687, https://doi.org/10.1016/j.jeurceramsoc.2018.11.013.

[2] S.L. Sing, W.Y. Yeong, F.E. Wiria, B.Y. Tay, Z. Zhao, L. Zhao, Z. Tian, S. Yang, Direct selective laser sintering and melting of ceramics: a review, Rapid Prototyp. J. 23 (2017) 611–623, https://doi.org/10.1108/RPJ-11-2015-0178.

[3] C.R. Deckard, Method and apparatus for producing parts BY selective sintering, 4,863,538, n.d.

[4] C.R. Deckard, SELECTIVE LASER SINTERING WITH LASERWISE CROSS-SCANNING, B23K 26/00, n.d.

[5] C.R. Deckard, Apparatus for producing parts BY selective sintering, 5,597,589, n.d.

[6] A. Lindstrom, Selective laser sintering, birth of an industry. me.utexas.edu/news/news/selective-laser-sintering-birth-of-an-industry, 2012. (Accessed 3 June 2020).

[7] H.L. Marcus, J.W. Barlow, J.J. Beaman, Selective laser sintering OF metals and ceramics, Int. J. Powder Metall. (1992) p.369–381.

[8] J.C. Nelson, N.K. Vail, J.W. Barlow, J.J. Beaman, D.L. Bourell, H.L. Marcus, Selective laser sintering of polymer-coated silicon carbide powders, Ind. Eng. Chem. Res. 34 (1995) 1641–1651, https://doi.org/10.1021/ie00044a017.

[9] A. Zocca, P. Colombo, C.M. Gomes, J. Günster, Additive manufacturing of ceramics: issues, potentialities, and opportunities, J. Am. Ceram. Soc. 98 (2015) 1983–2001, https://doi.org/10.1111/jace.13700.

[10] L. Ferrage, G. Bertrand, P. Lenormand, D. Grossin, B. Ben-Nissan, A review of the additive manufacturing (3DP) of bioceramics: alumina, zirconia (PSZ) and hydroxyapatite, J. Australas. Ceram. Soc. 53 (2017) 11–20, https://doi.org/10.1007/s41779-016-0003-9.

[11] L.C. Hwa, S. Rajoo, A.M. Noor, N. Ahmad, M.B. Uday, Recent advances in 3D printing of porous ceramics: a review, Curr. Opin, Solid State Mater. Sci. 21 (2017) 323–347, https://doi.org/10.1016/j.cossms.2017.08.002.

[12] S.L. Sing, W.Y. Yeong, F.E. Wiria, B.Y. Tay, Z. Zhao, L. Zhao, Z. Tian, S. Yang, Direct selective laser sintering and melting of ceramics: a review, Rapid Prototyp. J. 23 (2017) 611–623, https://doi.org/10.1108/RPJ-11-2015-0178.

[13] R. Galante, C.G. Figueiredo-Pina, A.P. Serro, Additive manufacturing of ceramics for dental applications: a review, Dent. Mater. 35 (2019) 825–846, https://doi.org/10.1016/j.dental.2019.02.026.

[14] Z. Chen, Z. Li, J. Li, C. Liu, C. Lao, Y. Fu, C. Liu, Y. Li, P. Wang, Y. He, 3D printing of ceramics: a review, J. Eur. Ceram. Soc. 39 (2019) 661–687, https://doi.org/10.1016/j.jeurceramsoc.2018.11.013.

[15] D.G.R. William D. Callister, Material Science and Engineering an Introduction, Eight Edition, n.d.

[16] B. Stevinson, D.L. Bourell, J.J. Beaman, Over-infiltration mechanisms in selective laser sintered Si/SiC preforms, Rapid Prototyp. J. 14 (2008) 149–154, https://doi.org/10.1108/13552540810878003.

[17] V. Bhavar, P. Kattire, V. Patil, S. Khot, K. Gujar, R. Singh, A Review on Powder Bed Fusion Technology of Metal Additive Manufacturing, in: A.B. Badiru, V.V. Valencia, D. Liu (Eds.), Addit. Manuf. Handb., first ed., CRC Press, 2017, pp. 251–253, https://doi.org/10.1201/9781315119106-15.

[18] J.J. Beaman, J.W. Barlow, D.L. Bourell, R.H. Crawford, H.L. Marcus, K.P. McAlea, Solid Freeform Fabrication: A New Direction in Manufacturing, Springer US, 1997, https://doi.org/10.1007/978-1-4615-6327-3. Boston, MA.

[19] J.-P. Kruth, G. Levy, F. Klocke, T.H.C. Childs, Consolidation phenomena in laser and powder-bed based layered manufacturing, CIRP Ann. 56 (2007) 730–759, https://doi.org/10.1016/j.cirp.2007.10.004.

[20] N.K. Tolochko, Y.V. Khlopkov, S.E. Mozzharov, M.B. Ignatiev, T. Laoui, V.I. Titov, Absorptance of powder materials suitable for laser sintering, Rapid Prototyp. J. 6 (2000) 155–161, https://doi.org/10.1108/13552540010337029.

[21] E. Juste, F. Petit, V. Lardot, F. Cambier, Shaping of ceramic parts by selective laser melting of powder bed, J. Mater. Res. 29 (2014) 2086–2094, https://doi.org/10.1557/jmr.2014.127.

[22] J. Liu, B. Zhang, C. Yan, Y. Shi, The effect of processing parameters on characteristics of selective laser sintering dental glass-ceramic powder, Rapid Prototyp. J. 16 (2010) 138–145, https://doi.org/10.1108/13552541011025861.

[23] S. Meyers, Additive Manufacturing of Technical Ceramics, (n.d.) 178.

[24] K. Shahzad, J. Deckers, J.-P. Kruth, J. Vleugels, Additive manufacturing of alumina parts by indirect selective laser sintering and post processing, J. Mater. Process. Technol. 213 (2013) 1484–1494, https://doi.org/10.1016/j.jmatprotec.2013.03.014.

[25] K.K.B. Hon, T.J. Gill, Selective laser sintering of SiC/polyamide composites, CIRP Ann. 52 (2003) 173–176, https://doi.org/10.1016/S0007-8506(07)60558-7.

[26] M. Schmid, F. Amado, G. Levy, K. Wegener, Flowability of Powders for Selective Laser Sintering (SLS) Investigated by Round Robin Test, in: P. da Silva Bártolo, A. de Lemos, A. Pereira, A. Mateus, C. Ramos, C. Santos, D. Oliveira, E. Pinto, F. Craveiro, H. da Rocha Terreiro Galha Bártolo, H. de Amorim Almeia, I. Sousa, J. Matias, L. Durão, M. Gaspar, N. Fernandes Alves, P. Carreira, T. Ferreira, T. Marques (Eds.), High Value Manuf. Adv. Res. Virtual Rapid Prototyp., CRC Press, 2013, pp. 95–99, https://doi.org/10.1201/b15961-19.

[27] A.B. Spierings, M. Voegtlin, T. Bauer, K. Wegener, Powder flowability characterisation methodology for powder-bed-based metal additive manufacturing, Prog. Addit. Manuf 1 (2016) 9–20, https://doi.org/10.1007/s40964-015-0001-4.

[28] M. Krantz, H. Zhang, J. Zhu, Characterization of powder flow: static and dynamic testing, Powder Technol. 194 (2009) 239–245, https://doi.org/10.1016/j.powtec.2009.05.001.

[29] H. Lu, X. Guo, Y. Liu, X. Gong, Effect of particle size on flow mode and flow characteristics of pulverized coal, KONA Powder Part. J. 32 (2015) 143–153, https://doi.org/10.14356/kona.2015002.

[30] L.X. Liu, I. Marziano, A.C. Bentham, J.D. Litster, E.T. White, T. Howes, Effect of particle properties on the flowability of ibuprofen powders, Int. J. Pharm. 362 (2008) 109–117, https://doi.org/10.1016/j.ijpharm.2008.06.023.

[31] X. Fu, D. Huck, L. Makein, B. Armstrong, U. Willen, T. Freeman, Effect of particle shape and size on flow properties of lactose powders, Particuology 10 (2012) 203–208, https://doi.org/10.1016/j.partic.2011.11.003.

[32] M.K. Stanford, C. Dellacorte, D. Eylon, Particle size effects on flow properties of Ps304 plasma spray feedstock powder blend, in: W.M. Kriven, H.-T. Lin (Eds.), Ceram. Eng. Sci. Proc., John Wiley & Sons, Inc., USA, Hoboken, NJ, 2003, pp. 577–585, https://doi.org/10.1002/9780470294802.ch82.

[33] D. Sofia, D. Barletta, M. Poletto, Flowability of ceramic powders in the sintering process, in: Jaipur (Rajasthan), Thapar University, India, 2016, p. 8.

[34] D. Sofia, R. Chirone, P. Lettieri, D. Barletta, M. Poletto, Selective laser sintering of ceramic powders with bimodal particle size distribution, Chem. Eng. Res. Des. 136 (2018) 536–547, https://doi.org/10.1016/j.cherd.2018.06.008.

[35] N.P. Karapatis, G. Egger, Optimization of powder layer density in selective laser sintering, in: AUSTIN, TX, 1999, p. 10.

[36] N.K. Tolochko, Y.V. Khlopkov, S.E. Mozzharov, M.B. Ignatiev, T. Laoui, V.I. Titov, Absorptance of powder materials suitable for laser sintering, Rapid Prototyp. J. 6 (2000) 155–161, https://doi.org/10.1108/13552540010337029.

[37] H.C.H. Ho, W.L. Cheung, I. Gibson, Effects of graphite powder on the laser sintering behaviour of polycarbonate, Rapid Prototyp. J. 8 (2002) 233–242, https://doi.org/10.1108/13552540210441148.

[38] T. Kamitani, O. Yamada, Y. Marutani, Selective laser sintering with heat of formation by using reactive materials, in: I. Miyamoto, K. Sugioka, T.W. Sigmon (Eds.), Omiya, Saitama, Japan, 2000, pp. 299–302, https://doi.org/10.1117/12.405683.

[39] J. Metelkova, Y. Kinds, K. Kempen, C. de Formanoir, A. Witvrouw, B. Van Hooreweder, On the influence of laser defocusing in Selective Laser Melting of 316L, Addit. Manuf 23 (2018) 161–169, https://doi.org/10.1016/j.addma.2018.08.006.

[40] T. Peng, C. Chen, Influence of energy density on energy demand and porosity of 316L stainless steel fabricated by selective laser melting, Int. J. Precis. Eng. Manuf.-Green Technol 5 (2018) 55–62, https://doi.org/10.1007/s40684-018-0006-9.

[41] K.G. Prashanth, S. Scudino, T. Maity, J. Das, J. Eckert, Is the energy density a reliable parameter for materials synthesis by selective laser melting? Mater. Res. Lett. 5 (2017) 386–390, https://doi.org/10.1080/21663831.2017.1299808.

[42] L. Thijs, K. Kempen, J.-P. Kruth, J. Van Humbeeck, Fine-structured aluminium products with controllable texture by selective laser melting of pre-alloyed AlSi10Mg powder, Acta Mater. 61 (2013) 1809–1819, https://doi.org/10.1016/j.actamat.2012.11.052.

[43] J. Suryawanshi, K.G. Prashanth, S. Scudino, J. Eckert, O. Prakash, U. Ramamurty, Simultaneous enhancements of strength and toughness in an Al-12Si alloy synthesized using selective laser melting, Acta Mater. 115 (2016) 285–294, https://doi.org/10.1016/j.actamat.2016.06.009.

[44] U. Scipioni Bertoli, A.J. Wolfer, M.J. Matthews, J.-P.R. Delplanque, J.M. Schoenung, On the limitations of volumetric energy density as a design parameter for selective laser melting, Mater. Des. 113 (2017) 331–340, https://doi.org/10.1016/j.matdes.2016.10.037.

[45] N. Eliaz, N. Metoki, Calcium phosphate bioceramics: a review of their history, structure, properties, coating technologies and biomedical applications, Materials 10 (2017) 334, https://doi.org/10.3390/ma10040334.

[46] T.A. Elkhooly, Preparation and characterization of calcium phosphate ceramics containing some rare earth oxides for using as biomaterials. https://doi.org/10.13140/rg.2.1.3902.5369, 2008.

[47] F.-C. Kao, P.-Y. Chiu, T.-T. Tsai, Z.-H. Lin, The application of nanogenerators and piezoelectricity in osteogenesis, Sci. Technol. Adv. Mater. 20 (2019) 1103–1117, https://doi.org/10.1080/14686996.2019.1693880.

[48] C. Colin, J.-D. Bartout, E. Shaker, OSSEOMATRIX PATENT - WO2014154901A1, WO2014154901A1, 2014.

[49] S. Ramesh, K.L. Aw, R. Tolouei, M. Amiriyan, C.Y. Tan, M. Hamdi, J. Purbolaksono, M.A. Hassan, W.D. Teng, Sintering properties of hydroxyapatite powders prepared using different methods, Ceram. Int. 39 (2013) 111–119, https://doi.org/10.1016/j.ceramint.2012.05.103.

[50] L. Hao, M.M. Savalani, Y. Zhang, K.E. Tanner, R.J. Heath, R.A. Harris, Characterization of selective laser-sintered hydroxyapatite-based biocomposite structures for bone replacement, Proc. R. Soc. Math. Phys. Eng. Sci. 463 (2007) 1857–1869, https://doi.org/10.1098/rspa.2007.1854.

[51] S. Eosoly, D. Brabazon, S. Lohfeld, L. Looney, Selective laser sintering of hydroxyapatite/poly-ε-caprolactone scaffolds, Acta Biomater. 6 (2010) 2511–2517, https://doi.org/10.1016/j.actbio.2009.07.018.

[52] Y. Xia, P. Zhou, X. Cheng, Y. Xie, C. Liang, C. Li, S. Xu, Selective laser sintering fabrication of nano-hydroxyapatite/poly-ε-caprolactone scaffolds for bone tissue engineering applications, Int. J. Nanomed. 8 (2013) 4197–4213, https://doi.org/10.2147/IJN.S50685.

[53] D.P. Minh, S. Rio, P. Sharrock, H. Sebei, N. Lyczko, N.D. Tran, M. Raii, A. Nzihou, Hydroxyapatite starting from calcium carbonate and orthophosphoric acid: synthesis, characterization, and applications, J. Mater. Sci. 49 (2014) p.4261–4269, https://doi.org/10.1007/s10853-014-8121-7.

[54] F. Cruz, Fabrication of HA/PLLA composite scaffolds for bone tissue engineering using additive manufacturing technologies, in: M. Elnashar (Ed.), Biopolymers, Sciyo, 2010, https://doi.org/10.5772/10264.

[55] H. Zeng, J.L. Pathak, Y. Shi, J. Ran, L. Liang, Q. Yan, T. Wu, Q. Fan, M. Li, Y. Bai, Indirect selective laser sintering-printed microporous biphasic calcium phosphate scaffold promotes endogenous bone regeneration via activation of ERK1/2 signaling, Biofabrication 12 (2020) 25032, https://doi.org/10.1088/1758-5090/ab78ed.

[56] C. Shuai, C. Gao, Y. Nie, H. Hu, H. Qu, S. Peng, Structural design and experimental analysis of a selective laser sintering system with nano-hydroxyapatite powder, J. Biomed. Nanotechnol. 6 (2010) 370–374, https://doi.org/10.1166/jbn.2010.1139.

[57] C. Shuai, C. Gao, Y. Nie, H. Hu, Y. Zhou, S. Peng, Structure and properties of nano-hydroxypatite scaffolds for bone tissue engineering with a selective laser sintering system, Nanotechnology 22 (2011), 285703, https://doi.org/10.1088/0957-4484/22/28/285703.

[58] C. Shuai, P. Li, J. Liu, S. Peng, Optimization of TCP/HAP ratio for better properties of calcium phosphate scaffold via selective laser sintering, Mater. Char. 77 (2013) 23–31, https://doi.org/10.1016/j.matchar.2012.12.009.

[59] L. Hao, M.M. Savalani, Y. Zhang, K.E. Tanner, R.J. Heath, R.A. Harris, Characterization of selective laser-sintered hydroxyapatite-based biocomposite structures for bone replacement, Proc. R. Soc. Math. Phys. Eng. Sci. 463 (2007) 1857–1869, https://doi.org/10.1098/rspa.2007.1854.

[60] K. Xiao, K.W. Dalgarno, D.J. Wood, R.D. Goodridge, C. Ohtsuki, Indirect selective laser sintering of apatite—wollastonite glass—ceramic, Proc. Inst. Mech. Eng. [H] 222 (2008) 1107–1114, https://doi.org/10.1243/09544119JEIM411.

[61] B. Duan, M. Wang, W.Y. Zhou, W.L. Cheung, Z.Y. Li, W.W. Lu, Three-dimensional nanocomposite scaffolds fabricated via selective laser sintering for bone tissue engineering, Acta Biomater. 6 (2010) 4495–4505, https://doi.org/10.1016/j.actbio.2010.06.024.

[62] L. Ferrage, Elaboration d'un assemblage céramique-métal par fusion/frittage sélectif(ve) d'un lit de poudre à l'aide d'un laser Nd :YAG, Université Toulouse III – Paul Sabatier, 2018.

[63] T. Kimoto, Fundamentals of Silicon Carbide Technology, (n.d.) 555.

[64] J.-C.N.G. Fantozzi, Guillaume Bonnefont, Les céramiques industrielles - propriétés, mise en forme et applications, Dunod (2013).

[65] K. Liu, T. Wu, D.L. Bourell, Y. Tan, J. Wang, M. He, H. Sun, Y. Shi, J. Chen, Laser additive manufacturing and homogeneous densification of complicated shape SiC ceramic parts, Ceram. Int. 44 (2018) 21067–21075, https://doi.org/10.1016/j.ceramint.2018.08.143.

[66] L. Jin, K. Zhang, T. Xu, T. Zeng, S. Cheng, The fabrication and mechanical properties of SiC/SiC composites prepared by SLS combined with PIP, Ceram. Int. 44 (2018) 20992–20999, https://doi.org/10.1016/j.ceramint.2018.08.134.

[67] B.R. Birmingham, H.L. Marcus, Solid Freeform Fabrication of Silicon Carbide Shapes by Selective Laser Reaction Sintering (SLRS), (n.d.) 9.

[68] W. Löschau, R. Lenk, S. Scharek, M. Teichgraber, S. Nowotny, C. Richter, Prototyping of complex-shaped parts and tools of Si/SiC-ceramics, Ind. Ceram. 38 (2000) 6, https://doi.org/10.1002/3527607293.ch24.

[69] P. Regenfuss, A. Streek, L. Hartwig, S. Klötzer, Th Brabant, M. Horn, R. Ebert, H. Exner, Principles of laser micro sintering, Rapid Prototyp. J. 13 (2007) 204–212, https://doi.org/10.1108/13552540710776151.

[70] A. Streek, P. Regenfuß, F. Ullmann, L. Hartwig, R. Ebert, H. Exner, PROCESSING OF SILICON CARBIDE BY LASER MICRO SINTERING, (n.d.) 10.

[71] S. Meyers, L. De Leersnijder, J. Vleugels, J.-P. Kruth, Direct laser sintering of reaction bonded silicon carbide with low residual silicon content, J. Eur. Ceram. Soc. 38 (2018) 3709–3717, https://doi.org/10.1016/j.jeurceramsoc.2018.04.055.

[72] S. Meyers, L.D. Leersnijder, J. Vleugels, J.-P. Kruth, Increasing the silicon carbide content in laser sintered reaction bonded silicon carbide, in: N.P. Bansal, R.H.R. Castro, M. Jenkins, A. Bandyopadhyay, S. Bose, A. Bhalla, J.P. Singh, M.M. Mahmoud, G. Pickrell, S. Johnson (Eds.), Ceram. Trans. Ser., John Wiley & Sons, Inc., USA, Hoboken, NJ, 2018, pp. 207–215, https://doi.org/10.1002/9781119423829.ch18.

[73] P. Stierlen, P. Eyerer, SilSiC..Ceranic Prototypes via LS21..Process (Liquid SiliconInfiltration of LaserSintered C..SiC Parts), (n.d.) 8.

[74] S. Song, Z. Gao, B. Lu, C. Bao, B. Zheng, L. Wang, Performance optimization of complicated structural SiC/Si composite ceramics prepared by selective laser sintering, Ceram. Int. 46 (2020) 568–575, https://doi.org/10.1016/j.ceramint.2019.09.004.

[75] N.K. Vailt, J.W. Barlow, H.L. Marcus, Silicon Carbide Preforms for Metal Infiltration by Selective Laser Sintering™ of Polymer Encapsulated Powders, (n.d.) 11.

[76] R.S. Evans, D.L. Bourell, J.J. Beaman, M.I. Campbell, Rapid manufacturing of silicon carbide composites, Rapid Prototyp. J. 11 (2005) 37–40, https://doi.org/10.1108/13552540510573374.

[77] R.S. Evans, D.L. Bourell, J.J. Beaman, M.I. Campbell, Reaction Bonded Silicon Carbide: SFF, Process Refinement and Applications, (n.d.) 10.

[78] B.Y. Stevinson, D.L. Bourell, J.J.B. Jr, SUPPORT-FREE INFILTRATION OF SELECTIVE LASER SINTERED (SLS) SILICON CARBIDE PREFORMS, (n.d.) 7.

[79] B.W. Xiong, H. Yu, Z.F. Xu, Q.S. Yan, Y.H. Zheng, P.L. Zhu, S.N. Chen, Study on dual binders for fabricating SiC particulate preforms using selective laser sintering, Compos. B Eng. 48 (2013) 129–133, https://doi.org/10.1016/j.compositesb.2012.09.092.

[80] J. Chevalier, What future for zirconia as a biomaterial? Biomaterials 27 (2006) 535–543, https://doi.org/10.1016/j.biomaterials.2005.07.034.

[81] S. Deville, J. Chevalier, G. Fantozzi, J.F. Bartolomé, J. Requena, J.S. Moya, R. Torrecillas, L.A. Diaz, Low-temperature ageing of zirconia-toughened alumina ceramics and its implication in biomedical implants, J. Eur. Ceram. Soc. 23 (2003) 2975–2982, https://doi.org/10.1016/S0955-2219(03)00313-3.

[82] The different forms OF zirconia, in: Zirconia, Elsevier, 1992, pp. 12–16, https://doi.org/10.1016/B978-1-4831-7819-6.50005-9.

[83] F.P. Shepard, N.F. Marshall, P.A. Mcloughlin, Pulsating turbidity currents with relationship to high swell and high tides, Nature 258 (1975) 704–706, https://doi.org/10.1038/258704a0.

[84] O. Ruff, F. Ebert, E. Stephan, Beiträge zur Keramik hochfeuerfester Stoffe II. Das System ZrO2?CaO, Z. Fär Anorg, Allg. Chem. 180 (1929) 215–224, https://doi.org/10.1002/zaac.19291800122.

[85] E.W. Leib, U. Vainio, R.M. Pasquarelli, J. Kus, C. Czaschke, N. Walter, R. Janssen, M. Müller, A. Schreyer, H. Weller, T. Vossmeyer, Synthesis and thermal stability of zirconia and yttria-stabilized zirconia microspheres, J. Colloid Interface Sci. 448 (2015) 582–592, https://doi.org/10.1016/j.jcis.2015.02.049.

[86] R. Benzaid, J. Chevalier, M. Saâdaoui, G. Fantozzi, M. Nawa, L.A. Diaz, R. Torrecillas, Fracture toughness, strength and slow crack growth in a ceria stabilized zirconia–alumina nanocomposite for medical applications, Biomaterials 29 (2008) 3636–3641, https://doi.org/10.1016/j.biomaterials.2008.05.021.

[87] P. Kohorst, L. Borchers, J. Strempel, M. Stiesch, T. Hassel, F.-W. Bach, C. Hübsch, Low-temperature degradation of different zirconia ceramics for dental applications, Acta Biomater. 8 (2012) 1213–1220, https://doi.org/10.1016/j.actbio.2011.11.016.

[88] Ph Bertrand, F. Bayle, C. Combe, P. Goeuriot, I. Smurov, Ceramic components manufacturing by selective laser sintering, Appl. Surf. Sci. 254 (2007) 989–992, https://doi.org/10.1016/j.apsusc.2007.08.085.

[89] I. Shishkovsky, I. Yadroitsev, Ph Bertrand, I. Smurov, Alumina–zirconium ceramics synthesis by selective laser sintering/melting, Appl. Surf. Sci. 254 (2007) 966–970, https://doi.org/10.1016/j.apsusc.2007.09.001.

[90] J. Wilkes, Y. Hagedorn, W. Meiners, K. Wissenbach, Additive manufacturing of ZrO2-Al2O3 ceramic components by selective laser melting, Rapid Prototyp. J. 19 (2013) 51–57, https://doi.org/10.1108/13552541311292736.

[91] S.M. Lakiza, JaS. Tyschenko, L.M. Lopato, Phase diagram of the Al2O3–HfO2–Y2O3 system, J. Eur. Ceram. Soc. 31 (2011) 1285–1291, https://doi.org/10.1016/j.jeurceramsoc.2010.04.041.

[92] Y.-C. Hagedorn, J. Wilkes, W. Meiners, W. Konrad, R. Poprawe, 6 Proc. Lane 2010 Part 2, Net Shaped High Performance Oxide Ceramic Parts by Selective Laser Melting, Laser Assist. Net Shape Eng, vol. 5, 2010, pp. 587–594, https://doi.org/10.1016/j.phpro.2010.08.086.

[93] Q. Liu, Y. Danlos, B. Song, B. Zhang, S. Yin, H. Liao, Effect of high-temperature preheating on the selective laser melting of yttria-stabilized zirconia ceramic, J. Mater. Process. Technol. 222 (2015) 61–74, https://doi.org/10.1016/j.jmatprotec.2015.02.036.

[94] L. Ferrage, G. Bertrand, P. Lenormand, Dense yttria-stabilized zirconia obtained by direct selective laser sintering, Addit. Manuf 21 (2018) 472–478, https://doi.org/10.1016/j.addma.2018.02.005.

[95] J. Koopmann, J. Voigt, T. Niendorf, Additive manufacturing of a steel–ceramic multi-material by selective laser melting, Metall. Mater. Trans. B 50 (2019) 1042–1051, https://doi.org/10.1007/s11663-019-01523-1.

[96] F. Verga, M. Borlaf, L. Conti, K. Florio, M. Vetterli, T. Graule, M. Schmid, K. Wegener, Laser-based powder bed fusion of alumina toughened zirconia, Addit. Manuf. 31 (2020), 100959, https://doi.org/10.1016/j.addma.2019.100959.

[97] K. Shahzad, J. Deckers, Z. Zhang, J.-P. Kruth, J. Vleugels, Additive manufacturing of zirconia parts by indirect selective laser sintering, J. Eur. Ceram. Soc. 34 (2014) 81–89, https://doi.org/10.1016/j.jeurceramsoc.2013.07.023.

[98] F. Chen, J.-M. Wu, H.-Q. Wu, Y. Chen, C.-H. Li, Y.-S. Shi, Microstructure and mechanical properties of 3Y-TZP dental ceramics fabricated by selective laser sintering combined with cold isostatic pressing, Int. J. Lightweight Mater. Manuf 1 (2018) 239–245, https://doi.org/10.1016/j.ijlmm.2018.09.002.

[99] Y. Shi, Additive manufacturing of zirconia parts via selective laser sintering combined with cold isostatic pressing, J. Mech. Eng. 50 (2014) 118, https://doi.org/10.3901/JME.2014.21.118.

[100] C.B. Carter, M.G. Norton, Ceramic Materials, Springer New York, 2013, https://doi.org/10.1007/978-1-4614-3523-5. New York, NY.

[101] Aluminum facts, Gov. Can. https://www.nrcan.gc.ca/our-natural-resources/minerals-mining/aluminum-facts/20510, 2019. (Accessed 7 September 2020).

[102] Y. Zheng, K. Zhang, T.T. Liu, W.H. Liao, C.D. Zhang, H. Shao, Cracks of alumina ceramics by selective laser melting, Ceram. Int. 45 (2019) 175–184, https://doi.org/10.1016/j.ceramint.2018.09.149.

[103] P.K. Subramanian, H.L. Marcus, Selective laser sintering of alumina using aluminum binder, Mater. Manuf. Process. 10 (1995) 689–706, https://doi.org/10.1080/10426919508935060.

[104] K. Subramanian, N. Vail, J. Barlow, H. Marcus, Selective laser sintering of alumina with polymer binders, Rapid Prototyp. J. 1 (1995) 24–35, https://doi.org/10.1108/13552549510086844.

[105] I.S. Lee, Full densed alumina-glass composites by SLS and ceracon forging process, Met. Mater 3 (1997) 203–209, https://doi.org/10.1007/BF03025964.

[106] H. Yves-Christian, W. Jan, M. Wilhelm, W. Konrad, P. Reinhart, Net shaped high performance oxide ceramic parts by selective laser melting, Phys. Procedia 5 (2010) 587–594, https://doi.org/10.1016/j.phpro.2010.08.086.

[107] K. Liu, C.H. Li, W.T. He, Y.S. Shi, J. Liu, Investigation on indirect selective laser sintering alumina ceramic parts combined with cold isostatic pressing, Appl. Mech. Mater. 217–219 (2012) 2217–2221. 10.4028/www.scientific.net/AMM.217-219.2217.

[108] J. Deckers, J.-P. Kruth, K. Shahzad, J. Vleugels, Density improvement of alumina parts produced through selective laser sintering of alumina-polyamide composite powder, CIRP Ann. 61 (2012) 211–214, https://doi.org/10.1016/j.cirp.2012.03.032.

[109] J. Deckers, J.-P. Kruth, L. Cardon, K. Shahzad, J. Vleugels, Densification and geometrical assessments of alumina parts produced through indirect selective laser sintering of alumina-polystyrene composite powder, stroj. Vestn. J. Mech. Eng. 59 (2013), https://doi.org/10.5545/sv-jme.2013.998.

[110] J. Deckers, K. Shahzad, J. Vleugels, J.P. Kruth, Isostatic pressing assisted indirect selective laser sintering of alumina components, Rapid Prototyp. J. 18 (2012) 409–419, https://doi.org/10.1108/13552541211250409.

[111] K. Liu, Y. Shi, W. He, C. Li, Q. Wei, J. Liu, Densification of alumina components via indirect selective laser sintering combined with isostatic pressing, Int. J. Adv. Manuf. Technol. 67 (2013) 2511–2519, https://doi.org/10.1007/s00170-012-4668-0.

[112] M. Huang, D.Q. Zhang, Z.H. Liu, J. Yang, F. Duan, C.K. Chua, S.C. Lim, M.S. Yip, Comparison study of fabrication of ceramic rotor using various manufacturing methods, Ceram. Int. 40 (2014) 12493–12502, https://doi.org/10.1016/j.ceramint.2014.04.104.

[113] S.-S. Liu, M. Li, J.-M. Wu, A.-N. Chen, Y.-S. Shi, C.-H. Li, Preparation of high-porosity Al2O3 ceramic foams via selective laser sintering of Al2O3 poly-hollow microspheres, Ceram. Int. 46 (2020) 4240–4247, https://doi.org/10.1016/j.ceramint.2019.10.144.

[114] I.S. Lee, Development of monoclinic HBO2 as an inorganic binder for SLS of alumina powder, J. Mater. Sci. Lett. 17 (1998) 1321–1324, https://doi.org/10.1023/A:1006648701389.

[115] I. Lee, Densification of porous Al2O3-Al4B2O9 ceramic composites fabricated by SLS process, J. Mater. Sci. Lett. 18 (1999) 1557–1561, https://doi.org/10.1023/A:1006695829140.

[116] I. Lee, Infiltration of alumina sol into SLS processed porous Al2O3-Al4B2O9 ceramic composites, J. Mater. Sci. Lett. 20 (2001) 223–226, https://doi.org/10.1023/A:1006790416275.

[117] I. Lee, Influence of heat treatment upon SLS processed composites fabricated with alumina and monoclinic HBO2, J. Mater. Sci. Lett. 21 (2002) 209–212, https://doi.org/10.1023/A:1014756724160.

[118] J. Wilkes, Y. Hagedorn, W. Meiners, K. Wissenbach, Additive manufacturing of ZrO2-Al2O3 ceramic components by selective laser melting, Rapid Prototyp. J. 19 (2013) 51–57, https://doi.org/10.1108/13552541311292736.

[119] K. Shahzad, J. Deckers, S. Boury, B. Neirinck, J.-P. Kruth, J. Vleugels, Preparation and indirect selective laser sintering of alumina/PA microspheres, Ceram. Int. 38 (2012) 1241–1247, https://doi.org/10.1016/j.ceramint.2011.08.055.

[120] P. Deckers, A. de Lemos, A. Tojeira, A. Pereira, A. Mateus, A. Mendes, C. dos Santos, D. Freitas, H. Bártolo, H. Almeida, I. dos Reis, J. Dias, M. Domingos, N. Alves, R. Pereira, T. Patrício, T. Ferreira (Eds.), Production of Alumina Parts through Selective Laser Sintering of Alumina-Polyamide Composite Powder, CRC Press, 2011, https://doi.org/10.1201/b11341.

[121] L. Cardon, J. Deckers, A. Verberckmoes, K. Ragaert, L. Delva, K. Shahzad, J. Vleugels, J.-P. Kruth, Polystyrene-coated alumina powder via dispersion polymerization for indirect selective laser sintering applications, J. Appl. Polym. Sci. (2012), https://doi.org/10.1002/app.38388.

[122] R.-Z. Liu, P. Chen, J.-M. Wu, S. Chen, A.-N. Chen, J.-Y. Chen, S.-S. Liu, Y.-S. Shi, C.-H. Li, Effects of B4C addition on the microstructure and properties of porous alumina ceramics fabricated by direct selective laser sintering, Ceram. Int. 44 (2018) 19678–19685, https://doi.org/10.1016/j.ceramint.2018.07.220.

[123] K. Zhang, T. Liu, W. Liao, C. Zhang, Y. Yan, D. Du, Influence of laser parameters on the surface morphology of slurry-based Al$_2$O$_3$ parts produced through selective laser melting, Rapid Prototyp. J. 24 (2018) 333–341, https://doi.org/10.1108/RPJ-12-2016-0201.

[124] S.M. Nazemosadat, E. Foroozmehr, M. Badrossamay, Preparation of alumina/polystyrene core-shell composite powder via phase inversion process for indirect selective laser sintering applications, Ceram. Int. 44 (2018) 596–604, https://doi.org/10.1016/j.ceramint.2017.09.218.

[125] Z. Fan, M. Lu, H. Huang, Selective laser melting of alumina: a single track study, Ceram. Int. 44 (2018) 9484–9493, https://doi.org/10.1016/j.ceramint.2018.02.166.

[126] Y. Zou, C.-H. Li, J.-A. Liu, J.-M. Wu, L. Hu, R.-F. Gui, Y.-S. Shi, Towards fabrication of high-performance Al2O3 ceramics by indirect selective laser sintering based on particle packing optimization, Ceram. Int. 45 (2019) 12654–12662, https://doi.org/10.1016/j.ceramint.2019.02.203.

[127] T. Tsunoyama, M. Yoshida, A. Shimosaka, Y. Shirakawa, Effects of mixing ratio and order of admixed particles with two diameters on improvement of compacted packing fraction, Adv. Powder Technol. 31 (2020) 2430–2437, https://doi.org/10.1016/j.apt.2020.04.005.

[128] H. Chen, Y. Chen, Y. Liu, Q. Wei, Y. Shi, W. Yan, Packing quality of powder layer during counter-rolling-type powder spreading process in additive manufacturing, Int. J. Mach. Tool Manufact. 153 (2020), 103553, https://doi.org/10.1016/j.ijmachtools.2020.103553.

[129] Z. Snow, R. Martukanitz, S. Joshi, On the development of powder spreadability metrics and feedstock requirements for powder bed fusion additive manufacturing, Addit. Manuf 28 (2019) 78–86, https://doi.org/10.1016/j.addma.2019.04.017.

[130] T.M. Wischeropp, C. Emmelmann, M. Brandt, A. Pateras, Measurement of actual powder layer height and packing density in a single layer in selective laser melting, Addit. Manuf 28 (2019) 176–183, https://doi.org/10.1016/j.addma.2019.04.019.

[131] D. Gu, Y. Yang, L. Xi, J. Yang, M. Xia, Laser absorption behavior of randomly packed powder-bed during selective laser melting of SiC and TiB2 reinforced Al matrix composites, Optic Laser. Technol. 119 (2019), 105600, https://doi.org/10.1016/j.optlastec.2019.105600.

[132] J. Muñiz-Lerma, A. Nommeots-Nomm, K. Waters, M. Brochu, A comprehensive approach to powder feedstock characterization for powder bed fusion additive manufacturing: a case study on AlSi7Mg,, Materials 11 (2018) 2386, https://doi.org/10.3390/ma11122386.

[133] V.D. Khramtsov, The packing density of the particles in powder mixtures of different dispersities, Russ, J. Non-Ferr. Met 50 (2009) 294–297, https://doi.org/10.3103/S1067821209030213.

[134] Y. Bai, G. Wagner, C.B. Williams, Effect of particle size distribution on powder packing and sintering in binder jetting additive manufacturing of metals, J. Manuf. Sci. Eng. 139 (2017), 81019, https://doi.org/10.1115/1.4036640.

[135] L. Ferrage, G. Bertrand, P. Lenormand, Dense yttria-stabilized zirconia obtained by direct selective laser sintering, Addit. Manuf 21 (2018) 472–478, https://doi.org/10.1016/j.addma.2018.02.005.

[136] X. Lu, D.K. Schreiber, J.J. Neeway, J.V. Ryan, J. Du, Effects of optical dopants and laser wavelength on atom probe tomography analyses of borosilicate glasses, J. Am. Ceram. Soc. 100 (2017) 4801–4815, https://doi.org/10.1111/jace.14987.

[137] N.K. Tolochko, Y.V. Khlopkov, S.E. Mozzharov, M.B. Ignatiev, T. Laoui, V.I. Titov, Absorptance of powder materials suitable for laser sintering, Rapid Prototyp. J. 6 (2000) 155–161, https://doi.org/10.1108/13552540010337029.

[138] L. Ferrage, Elaboration d'un assemblage céramique-métal par fusion/frittage sélectif(ve) d'un lit de poudre à l'aide d'un laser Nd :YAG, 2018.

[139] N. Yılmaz, M.Y. Kayacan, Effect of single and multiple parts manufacturing on temperature-induced residual stress problems in SLM, Int. J. Material Form. (2020), https://doi.org/10.1007/s12289-020-01560-1.

[140] M.A. Doubenskaia, I.V. Zhirnov, V.I. Teleshevskiy, P. Bertrand, I.Y. Smurov, Determination of true temperature in selective laser melting of metal powder using infrared camera, Mater. Sci. Forum 834 (2015) 93–102. 10.4028/www.scientific.net/MSF.834.93.

[141] I. Smurov, M. Doubenskaia, Temperature Monitoring by Optical Methods in Laser Processing, in: J.D. Majumdar, I. Manna (Eds.), Laser-Assist. Fabr. Mater., Springer Berlin Heidelberg, Berlin, Heidelberg, 2013, pp. 375–422, https://doi.org/10.1007/978-3-642-28359-8_9.

[142] European Patent Office (EPO), Patents and Additive Manufacturing, 2020.

[143] N.K. Roy, D. Behera, O.G. Dibua, C.S. Foong, M.A. Cullinan, A novel microscale selective laser sintering (μ-SLS) process for the fabrication of microelectronic parts, Microsyst. Nanoeng. 5 (2019) 64, https://doi.org/10.1038/s41378-019-0116-8.

[144] N.K. Roy, A. Yuksel, M.A. Cullinan, S. Foong, MICRO - SELECTIVE SINTERING LASER SYSTEMS AND METHODS THEREOF, US 2018/0065186 A1, 2018.

[145] Christian von Burg, Niederteufen ( CH ), ADDITIVE MANUFACTURING DEVICE with A HEATING DEVICE, US 2018/0085998 A1, 2018.

[146] J. Zeltner, ADDITIVE MANUFACTURING DEVICE INCLUDING A MOVABLE BEAM GENERATION UNIT OR DIRECTING UNIT, US 2019/0315063 A1, 2019.

[147] D. Solenicki, U.S. Cl, ADDITIVE MANUFACTURING DEVICE COMPRISING A REPLACEABLE RAW MATERIAL PROCESSING UNIT, US 2019/0263064 A1, 2019.